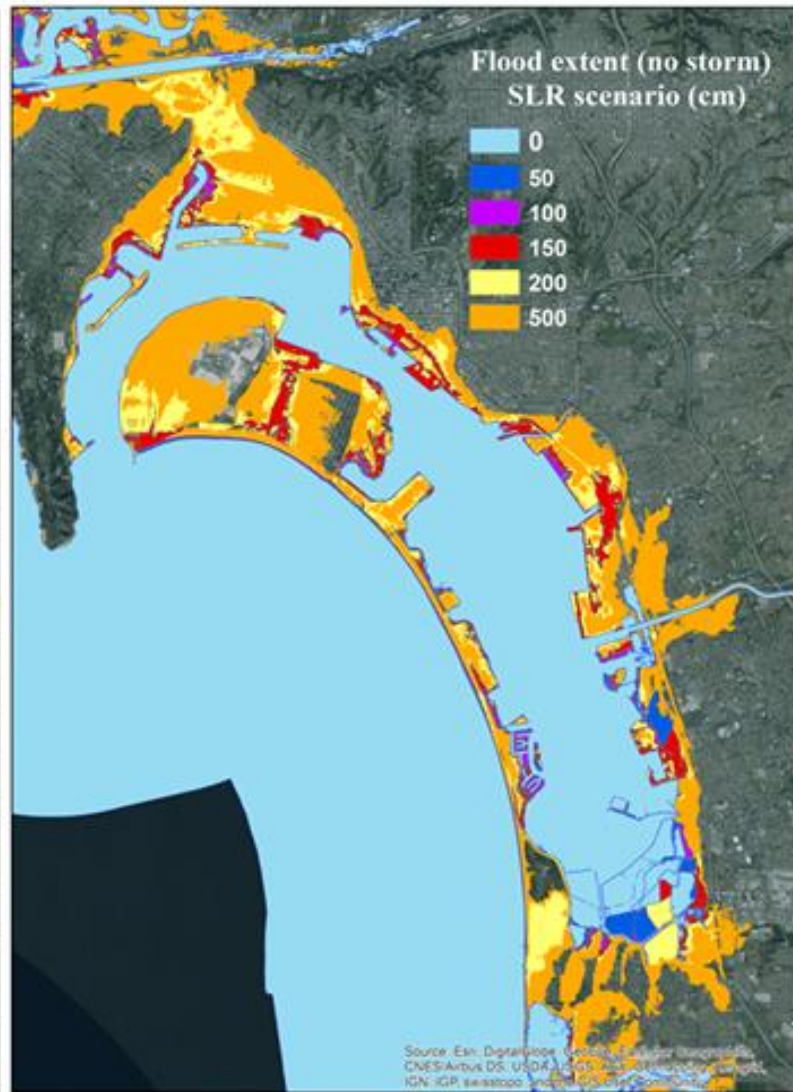
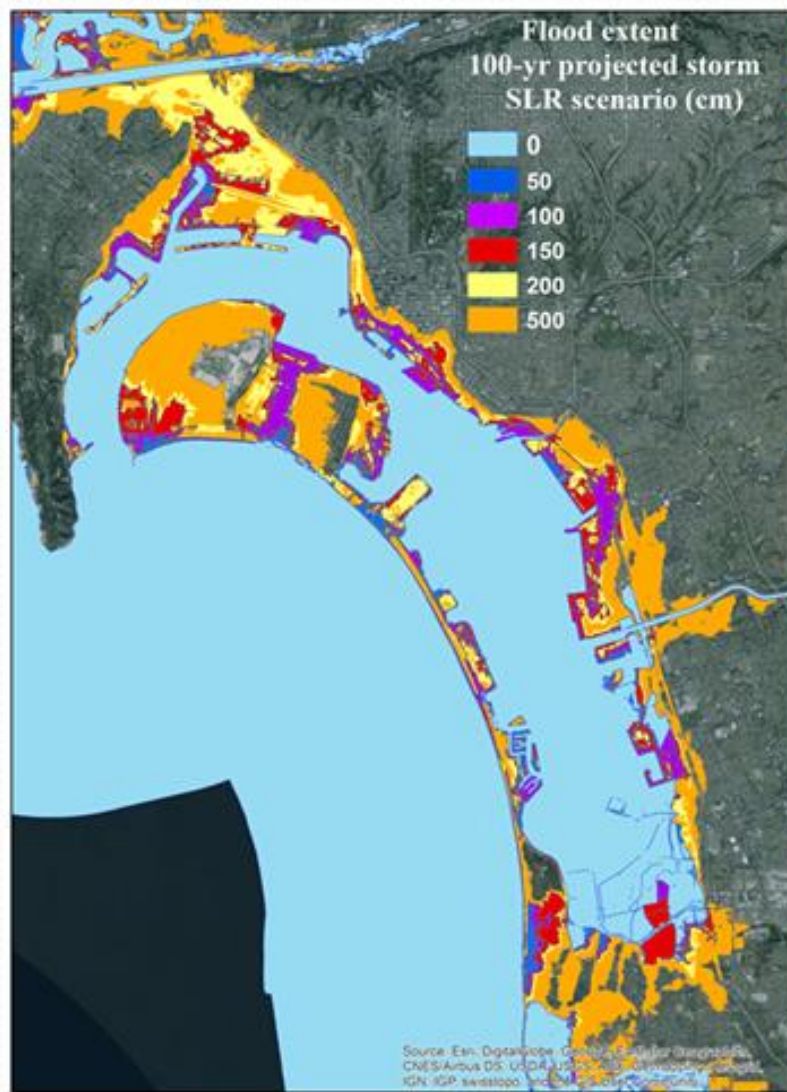


DOCKETED

Docket Number:	15-AFC-01
Project Title:	Puente Power Project
TN #:	216610
Document Title:	Recently published technical document for CoSMoS (Coastal Storm Modeling System), Version 3.
Description:	This technical report summarizes data and methods used to develop CoSMoS version 3.0 and its application to the approximately 480 km shoreline extending from the U.S. / Mexico border to Point Conception, CA.
Filer:	Mike Monasmith
Organization:	California Energy Commission
Submitter Role:	Commission Staff
Submission Date:	3/20/2017 1:00:44 PM
Docketed Date:	3/20/2017

Coastal Storm Modeling System (CoSMoS)



**CoSMoS v3.0 Phase 2 Southern California
Bight:
Summary of methods**

Table of Contents

2	
Executive Summary.....	33
Section 1. Study Area.....	44
Section 2. CoSMoS 3.0 model overview.....	55
Section 3. Models and data.....	88
3.1 Global scale wave model.....	88
Grids, model settings, and bathymetry.....	88
Boundary forcing.....	88
3.2 Regional scale wave and hydrodynamic model - Tier I.....	99
Grids, model settings, and bathymetry.....	99
Boundary forcing.....	1010
3.3 Local scale 2D wave and hydrodynamic model – Tier II.....	12
Grids, model settings, bathymetry and topography.....	12
Boundary forcing.....	14
3.4 Local scale 1D wave and hydrodynamic model – Tier III.....	15
Grids, model settings, bathymetry and topography.....	15
Boundary forcing.....	16
3.5 Long-term morphodynamic change models.....	16
3.6 Fluvial discharge model.....	1919
Peak discharge rates.....	20
Idealized hydrograph.....	22
Section 4. Identification of storm events.....	23
Section 5. Scenarios and timing of events.....	26
Section 6. Determination of flood extents and uncertainty estimates.....	26
Acknowledgements.....	2929
References.....	2929
Appendix A: Downloadable data files.....	33
Appendix B: Abbreviations, figures, and tables.....	35

CoSMoS 3.0 Phase 2 Southern California Bight: Summary of data and methods

By Li H. Erikson, Patrick L. Barnard, Andrea C. O'Neill, Sean Vitousek, Patrick Limber, Amy C. Foxgrover, Liv M. Herdman, and Jonathan Warrick

Suggested citation:

Erikson, L.H., Barnard, P.L., O'Neill, A.C., Vitousek, S., Limber, P., Foxgrover, A.C., Herdman, L.H., and Warrick, J., 2017. CoSMoS 3.0 Phase 2 Southern California Bight: Summary of data and methods. U.S. Geological Survey. <http://dx.doi.org/10.5066/F7T151Q4>

Executive Summary

Flood maps are regularly used for design, disaster, and hazard mitigation planning, but until relatively recently; little information exists on probable coastal flood hazards under conditions of climate change. Changes in atmospheric conditions, such as wind and pressure, can impart deviations in both magnitude and frequency of storm events compared to the past which, combined with sea-level rise (SLR) will affect coastal flood hazard projections.

With the aim of forecasting flood hazards, the USGS, in collaboration with Deltares, developed the Coastal Storm Modeling System (CoSMoS) for the Southern California Bight (Barnard and others, 2014; <http://cosmos.deltares.nl/SoCalCoastalHazards/index.html>). That first iteration of CoSMoS (version 1) focused on evaluating flood hazards associated with historical storms and two SLR scenarios; the system continues to run operationally for near-term forecasts of regional wave climate and water levels. The work presented here, extends upon the initial CoSMoS work to include 1) high resolution grids for better representation of harbors, lagoons, bays, estuaries, and overland flow, 2) fluvial discharges that might locally impede and amplify flooding associated with coastal storms, 3) long-term morphodynamic change integrated into the coastal flooding projections, 4) uncertainty associated with terrain models, numerical model errors and vertical land motion, and 5) alterations to coastal storm intensity and frequency associated with a changing climate.

This report summarizes data and methods used to develop CoSMoS version 3.0 and its application to the approximately 480 km shoreline extending from the U.S. / Mexico border to Point Conception, CA. CoSMoS 3.0 downscales 21st century ocean and coastal storms from the global to local scale. Winds, sea level pressures, and sea surface temperatures derived from global climate models, were used to compute waves, storm surges, and sea level anomalies, for the 21st century. From this projected time-series, multiple storm events for select return periods were identified along different sections of the coast; these were modeled in detail using a train of numerical models that account for the combined effects of storm intensity, direction, sea-level rise, astronomic tides, and long-term morphologic change.

A total of 40 scenarios were simulated and represent potential future flood hazards associated with 3 storms (1-year, 20-year, and 100-year) and a background atmospheric condition in combination with present day mean sea level and 9 additional SLR scenarios (0.25 meters (m) to 2 m at 0.25 m increments and 5 m). Results have been synthesized and are available for download as Google Earth kmz files,

ArcGIS shapefiles, or GeoTIFFs at http://walrus.wr.usgs.gov/coastal_processes/cosmos/socal3.0/index.html. See Appendix A for data and format descriptions of downloadable files. A tool for visualization, data analysis, and additional downloadable data is available at <http://ourcoastourfuture.org>.

Disclaimer: The data and maps included in these files are intended to improve flood hazard awareness and preparedness associated with climate change; however, they do not guarantee the safety of an individual or structure. The U.S. Geological Survey provides these maps as a planning tool but assumes no legal liability or responsibility resulting from the use of this information.

Section 1. Study Area

The Southern California Bight (SCB) extends from the U.S. / Mexican border northwestward to Point Conception and encompasses ~ 480 kilometers (km) of open coast shoreline, punctuated by river mouths, bays, lagoons, and estuaries (fig. 1). The coast hosts a complex mixture of beach settings variably backed by narrow to wide beaches, dunes, low to high cliffs, and urban infrastructure.

Tectonic controls along the Pacific and North American plate boundary has resulted in the region being fronted by a narrow continental shelf (< 20 kilometers, km), a series of islands (Channel Islands) that can shelter portions of the coastline from open ocean swell, and a highly irregular complex bathymetry that hosts a plethora of submerged seamounts, troughs, and canyons (Christensen and Yeats, 1992; Hogarth and others, 2007). The seamounts, knolls, canyons, and Channel Islands significantly alter the open ocean deep water wave climate to a more complicated nearshore wave field (O'Reilly and Guza, 1993; O'Reilly and others, 1999; Rogers and others, 2007; Adams and others, 2011). Swell dominate the nearshore wave energy, but locally generated wind-waves comprise ~40% of the total wave energy spectrum (Crosby, 2016).

Astronomic tides are mixed semidiurnal with a mean tide range of 1.12 m to 1.23 m depending on location within the SCB (National Oceanic and Atmospheric Administration, NOAA, 2016; stations 9410230, 9411340, 941070, and 9410840). Tides travel from southeast to northwest, with high tide taking ~30 minutes to transit from San Diego to Point Conception.

Measured sea level rise (SLR) rates range from 0.95 millimeters/year (mm/yr) to 2.22 mm/year amongst 6 tide gauges located within the SCB, each with >30 years of sea level measurements (NOAA, <https://tidesandcurrents.noaa.gov/sltrends/sltrends.html>, accessed November 2016). Extensive studies that incorporate observations and modeling of climate change-induced SLR, project an acceleration in the rate and that an upper extreme level of 2.88 m may be reached by the year 2100, with a median projection of 0.74 m and 1.37 m for the representative concentration pathway (RCP) 4.5 and RCP 8.5 scenarios, respectively (Cayan and others, 2016).

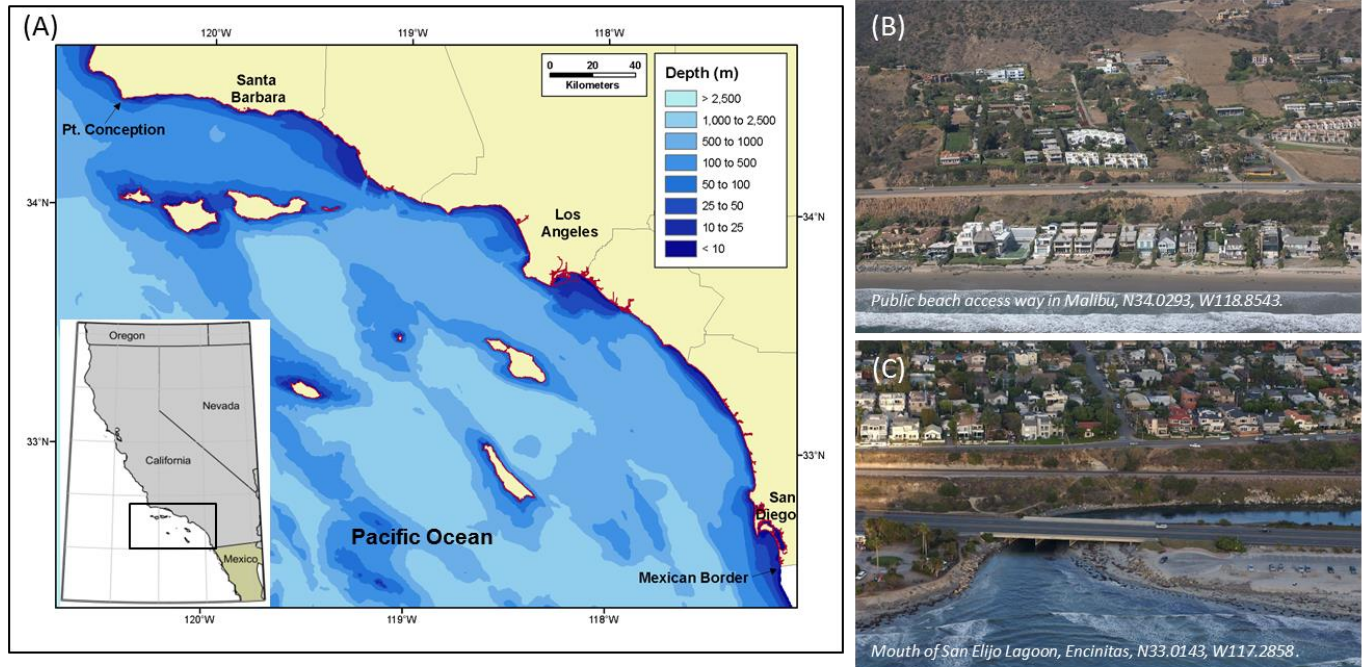


Figure 1. Map of study area and example photos of urbanized coastal sections. (A) Map of the Southern California Bight and bathymetry. (B and C) Images 200801843 and 200407620 downloaded from California Coastal Records Project, www.californiacoastline.org, copyright © 2002-2015 Kenneth & Gabrielle Adelman (last accessed December 2016).

Section 2. CoSMoS 3.0 model overview

CoSMoS 3.0 is comprised of one global scale wave model and a suite of regional and local scale models that simulate coastal hazards in response to projections of 21st century waves, storm surge, anomalous variations in water levels, river discharge, tides, and sea-level rise (table1; fig. 2). In CoSMoS 3.0 Phase 2, a total of 40 scenarios, resulting from the combination of 10 sea levels, 3 storm conditions, and one background condition were simulated. Sea-level rise ranged from 0 m to 2 m, at 0.25 m increments, plus an additional 5 m extreme. Future storm conditions represent the 1-year, 20-year, and 100-year return level coastal storm events, as derived and downscaled from winds, sea-level pressures (SLPs), and sea-surface temperatures (SSTs) of the RCP 4.5, GFDL-ESM2M global climate model (GCM).

Ocean waves, including both local seas and swell generated from distant storms across the Pacific Ocean, are the largest contributor to coastal flooding along the open coast of California during storm events. Thus, future wave conditions are first simulated with the global-scale WaveWatch III (WW3) model. Section 3.1 provides more detail on the global scale wave model.

Projected deep water waves computed with the global scale wave model are propagated to shore with a suite of regional (Tier I) and local (Tiers II and III) models that additionally simulate regional and local wave growth (seas) in combination with long-term and event-driven morphodynamic change and

water level changes due to astronomic tides, winds, sea-level pressure, steric effects, and sea-level rise (fig. 2).

Table 1. Models employed in CoSMoS.

Spatial scale	Model
Global scale	WaveWatch III
Regional scale (Tier I)	Delft3D FLOW and WAVE models
Local scale (Tier II)	Delft3D FLOW and WAVE models
Local scale (Tier III)	XBeach cross shore profile models

The regional Tier I model consists of one Delft3D hydrodynamic FLOW grid for computation of currents and water level variations (astronomic tides, storm surge, and steric effects) and one SWAN grid for computation of wave generation and propagation across the continental shelf. Wave conditions from the global wave model are applied at the open-boundaries of the SWAN model. The FLOW and SWAN models are two-way coupled so that tidal currents are accounted for in wave propagation and growth and conversely, that orbital velocities generated by waves impart changes on tidal currents. See Section 3.2 for more details on Tier I.

Employing high-resolution grids for fine-scale modeling of the entire study is not possible using desktop computers and therefore Tier II was segmented into 11 sections. Each sub-model consists of two SWAN grids and multiple FLOW grids. Wave and water level time-series of the Tier I model are applied at the open boundaries of each Tier II sub-model. See Section 3.3 and Section 3.5 for more details on Tier II.

Tier III consists of more than 4,000 cross-shore XBeach (eXtreme Beach) models that simulate event-driven morphodynamic change, water level variations, and infragravity wave runup every ~100 m alongshore. Wave runup is the maximum vertical extent of wave uprush on a beach or structure above the still water level, and in cases where infragravity waves exist, the reach of wave runup can be significantly further inland compared to wave runup driven by shorter incident waves (Roelvink and others, 2009). The U.S. west coast is particularly susceptible to infragravity wave runup due to the prevalence of breaking long-period swell (low wave steepness) across wide, mildly sloping (dissipative) beaches that result in a shoreward decay of incident wave energy and accompanying growth of infragravity energy.

In Phase 1 of CoSMoS 3.0, cross-shore profiles were extracted from a 2 meter (m) resolution seamless digital elevation model (DEM; USGS CoNED, 2016) and used as initial conditions for each of the >4,000 XBeach model runs, independent of the sea level scenario simulated. In Phase 2, long-term morphodynamic change resulting from SLR and changing wave conditions, was first modeled and used as initial conditions for each detailed flood simulation associated with the prescribed storm and SLR combinations. See Section 3.4 for more details on Tier III.

The methods and data presented in this report apply to both Phase 1 and 2 of CoSMoS version 3.0. Phase I differs from Phase II in that 1) long-term morphodynamic change was not included in the simulations and 2) only the 100-year storm (in combination with all SLR scenarios) was simulated.

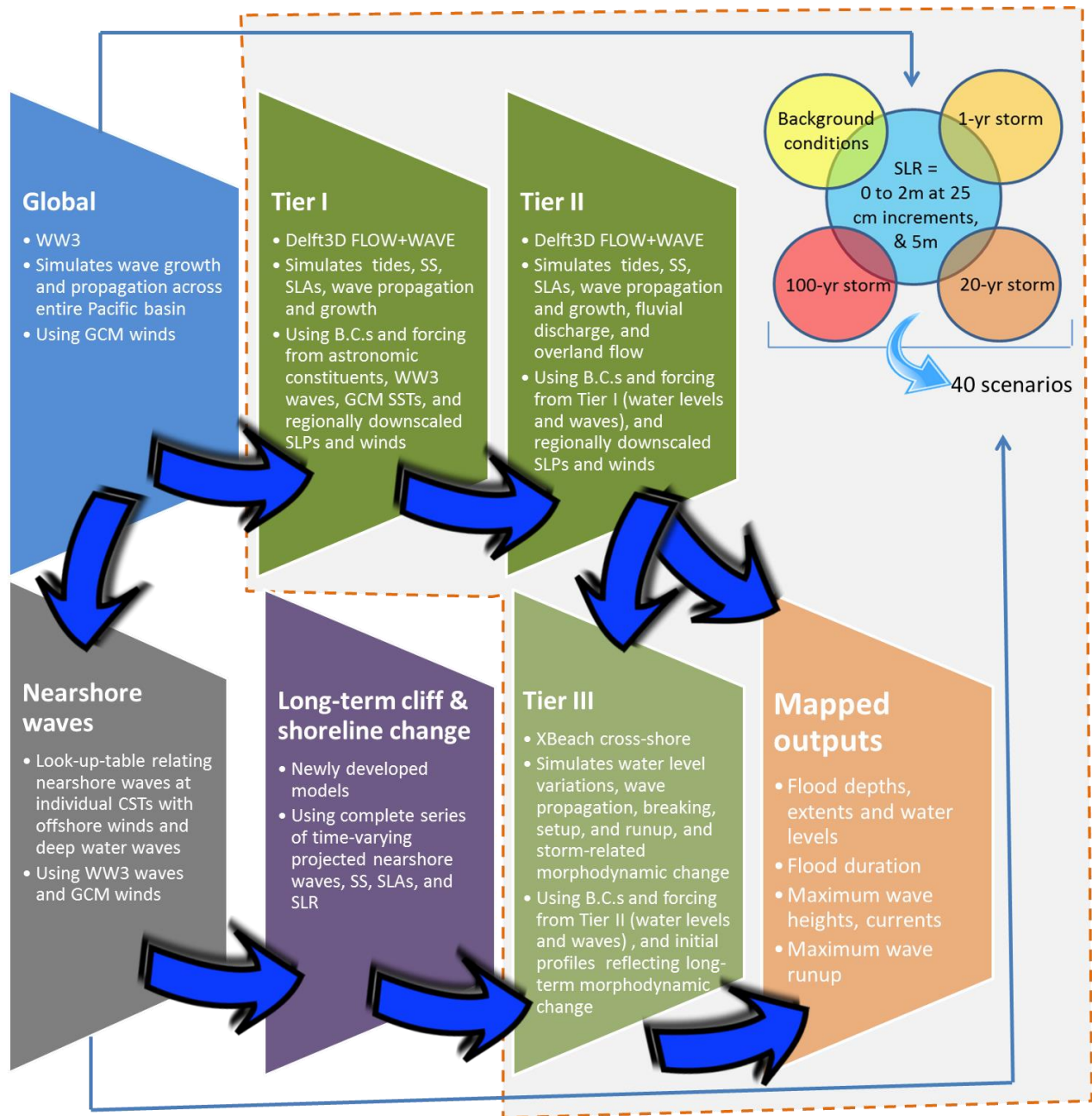


Figure 2. Schematic of CoSMoS version 3.0 Phase 2 numerical model approach for simulating coastal storm flooding under the influence of climate change. Each trapezoid represents individual components in the model train. Thin blue arrows denote the use of global climate data for *a priori* determination of coastal storm events; events were subsequently modeled in detail with Tiers I through III (grouped and shown with dashed line). The approach applies to CoSMoS version 3.0 Phase 1 as well, except that long-term morphodynamic change was not included and only the 100-year storm was simulated. Abbreviations: WW3: WaveWatch3; CST: cross shore transect; SLR: sea-level rise; SLP: sea-level pressure; GCM: global climate model; SLA: sea level anomalies; SS: storm surge; B.C.s: boundary conditions.

Section 3. Models and data

3.1 Global scale wave model

Grids, model settings, and bathymetry

The third-generation, spectral wave model WaveWatch III (WW3, version 3.14, Tolman, 2009) was used to project future wave conditions. The model was applied over a near-global grid (NWW3, latitude 80°S–80°N) with 1°x 1.25° spatial resolution, and a one-way nested Eastern North Pacific (ENP) grid with 0.25° spatial resolution (~27 km at latitude 37°N). Bathymetry and shoreline positions were populated with the 2-minute Naval Research Laboratory Digital Bathymetry Data Base (DBDB2) v3.0 and National Geophysical Data Center Global Self-Consistent Hierarchical High-Resolution Shoreline (GSHHS, Wessel and Smith, 2006). Wave spectra were computed with 15° directional resolution and 25 frequency bands ranging non-linearly from 0.04 to 0.5 Hz. Wind-wave growth and whitecapping was modeled with the Tolman and Chalikov (1996) source term package and nonlinear quadruplet wave interactions were computed with the Hasselmann and others (1985) formulation. Bulk wave parameter statistics (significant wave height, H_s ; peak wave period, T_p ; and peak wave direction, D_p) were saved hourly at points in deep water, offshore of the continental shelf. Time-series model outputs from a point coincident with the Scripps Institution of Oceanography California Data Information Program (CDIP) buoy 067 (33.221°N, 119.881°W) were used as deep water boundary conditions for running Tier I storm event and SLR scenarios for CoSMoS ver. 3.0.

Boundary forcing

Wind speeds and directions for years 2010 through 2100 computed with the National Oceanographic and Atmospheric Administration (NOAA) Geophysical Fluid Dynamics Laboratory earth systems global climate model (GCM) GFDL-ESM2M (Dunne and others, 2012; data download available at <http://nomads.gfdl.noaa.gov:8080/DataPortal/cmip5.jsp>) were used to drive the WW3 wave model. GFDL-ESM2M simulations employ coupling between global-scale atmosphere and ocean circulation models. The atmospheric component includes physical features such as aerosols (both natural and anthropogenic), cloud physics, precipitation, and evaporation; the oceanic model includes such processes as water fluxes, currents, sea ice dynamics and a representation of ocean mixing.

GFDL-ESM2M near-surface wind data are available at 10 m, neutrally stable fields on a 2.5° x 1.5° grid at a 3 hour time-step. Prior to running the WW3 model, east-west and north-south directed wind fields were linearly interpolated to the WW3 grid resolutions. The GFDL-ESM2M model was selected amongst the various GCMs available because 1) of the relatively high temporal model output resolution (3- hourly) of atmospheric fields, 2) the time-series included the entire 21st century as opposed to just the mid- and end-of century as was the case for most of the GCMs at the onset of the CoSMoS study, and 3) relatively good agreement between downscaled historical wave conditions compared to observations, particularly for the extreme events along this coastline (Erikson and others, 2015).

Whereas a complete time-series for the 21st century was modeled with WW3 and used for selection of storm events, deep water wave conditions for the mid- (2026-2045) and end-of-century (2081-2100) time-periods were also simulated and compared to the RCP 8.5 climate scenario. Comparisons between

modeled hind-casts (1976-2005) and the mid- and end- of century time-slices showed that for both climate scenarios, wave height is projected to slightly decrease offshore of Southern California and that a greater decrease is expected with RCP 8.5 (Erikson and others, 2015). Thus, this study was limited to the more conservative RCP 4.5, the climate scenario with likely higher future wave heights in the study area.

The climate scenarios were defined by the fifth phase of the Coupled Model Inter-comparison Project (CMIP5) and represent trajectories of increasing global radiative forcing that reach 4.5 W/m^2 and 8.5 W/m^2 by the year 2100, relative to pre-industrial (1850) radiative forcing (Hibbard and others, 2007). RCP 8.5 represents a high radiative forcing (Moss and others, 2010), and is roughly equivalent to the A2 emission scenarios of the IPCC CMIP3 Special Report on Emission Scenarios (SRES) (Meinshausen and others 2011). RCP 4.5 represents a scenario of medium radiative forcing with the onset of stabilization by mid-century, and is roughly equivalent to the B1 IPCC CMIP3 scenario.

3.2 Regional scale wave and hydrodynamic model - Tier I

Grids, model settings, and bathymetry

The WAVE and FLOW modules of the Delft3D version 4.01.00 were used to simulate waves and hydrodynamics, respectively. The WAVE module allows for two-way coupling (communication) between wave computations and FLOW hydrodynamics and simulates waves with the numerical model SWAN (Simulating Waves Nearshore, Delft University of Technology). SWAN is a commonly used third-generation spectral wave model specifically developed for nearshore wave simulations that account for propagation, refraction, dissipation, and depth-induced breaking (Booij and others, 1999; Ris, 1999). The SWAN model was run in a stationary mode, with settings identical to Rogers and others (2007): JONSWAP spectrum with peak enhancement factor of 3.3 at the open boundary forcing, 36 directional bins (i.e., 10° discretization), and 35 frequencies with logarithmic spacing from 0.0418 Hz to 1.00 Hz. Depth induced breaking was computed with the Battjes and Janssen (1978) formulation and a breaking index of 0.73; whitecapping is described with the default Komen and others (1994) expression. Bottom friction is based on the JONSWAP formulation, with the friction coefficient set at $0.067 \text{ m}^2/\text{s}$ (Hasselmann and others, 1973).

Delft3D-FLOW, developed by WL/Delft Hydraulics and Delft University of Technology, is a widely used numerical model that calculates non-steady flows and transport phenomena resulting from tidal and meteorological forcing (Lesser and others, 2004). The Tier I FLOW model was run with the following settings: water density equal to 1025 kg/m^3 , uniform Chezy bed roughness of 65, the Fredsoe stress formulation due to wave forces, a uniform horizontal viscosity of $1 \text{ m}^2/\text{s}$, and a linear wind drag model with coefficients of $6.3\text{e-}4$ and $7.2\text{e-}3$ at breakpoints of 0 m/s and 100 m/s wind speeds. FLOW models are run with a 30 second time-step and communication with the WAVE module every 20 minutes.

Tier I SWAN and FLOW models consist of identical structured curvilinear grids that extend from shore to ~200 km offshore in water depths $> 1,000 \text{ m}$ and range in resolution from $1.2 \text{ km} \times 2.5 \text{ km}$ in the nearshore to $3.5 \text{ km} \times 5 \text{ km}$ in the offshore. The two-way coupled model was run in a spherical coordinate system and with FLOW in a vertically-averaged mode (2DH). Bathymetry was derived from the National Geophysical Data Center (NGDC) Coastal Relief Model (<http://www.ngdc.noaa.gov/mgg/coastal/coastal.html>).

Boundary forcing

Tidal forcing

Spatially varying astronomic tidal amplitudes and phases derived from the Oregon State University (OSU) TOPEX/Poseidon global tide database (Egbert and others, 1994) were applied along all open boundaries of the Tier I FLOW grid. A total of 13 constituents were represented: M2, S2, N2, K2, K1, O1, P1, Q1, MF, MM, M4, MS4, and MN4.

Sea level anomalies

Sea level anomalies due to large-scale meteorological and oceanographic processes unrelated to storms, were applied along all open boundaries of the Tier I FLOW grid. Elevated sea-level anomalies (SLAs) are often observed in conjunction with El Niño events (Flick, 1998; Storlazzi and Griggs, 1998; Bromirski and others, 2003) and yield water levels of 10-20 cm above normal for several months (Cayan and others, 2008).

In an effort to maintain simplicity, correlations of SLAs with sea surface temperature anomalies (SSTAs) were developed. Both observed and GCM SSTAs are readily available (making it simple to use) and are physically linked to SLAs via direct correspondence to thermal expansion (i.e., thermosteric) and indirectly to changes in large scale wind patterns. SSTAs were computed by subtracting out the long term mean (1971 to 2000; Reynolds and others, 2002) from a satellite-derived SST time-series spanning the years 1981 through 2014 (NOAA/OAR/ESRL PSD). A linear least-square fit through the upper envelope of mean monthly SSTAs and SLAs measured at La Jolla resulted in the empirical equation ($r = 0.90$, fig. 3),

$$SLA = C_0 + C_1 \cdot SSTA \quad (3)$$

where the empirical coefficients C_0 and C_1 were found to equal 0.0546 and 0.0745, respectively. The upper envelope was defined by the maximum SLA within 0.25° SSTA bins from -2.0°C to $+2.5^\circ\text{C}$. A fit through the upper envelope, rather than all the data, was done ensuring a positive SLA for higher SSTAs. Due to scatter in the data and relatively small SLAs, a fit through all data would yield only a slight positive SLA (~ 0.10 m) for the maximum observed SSTA.

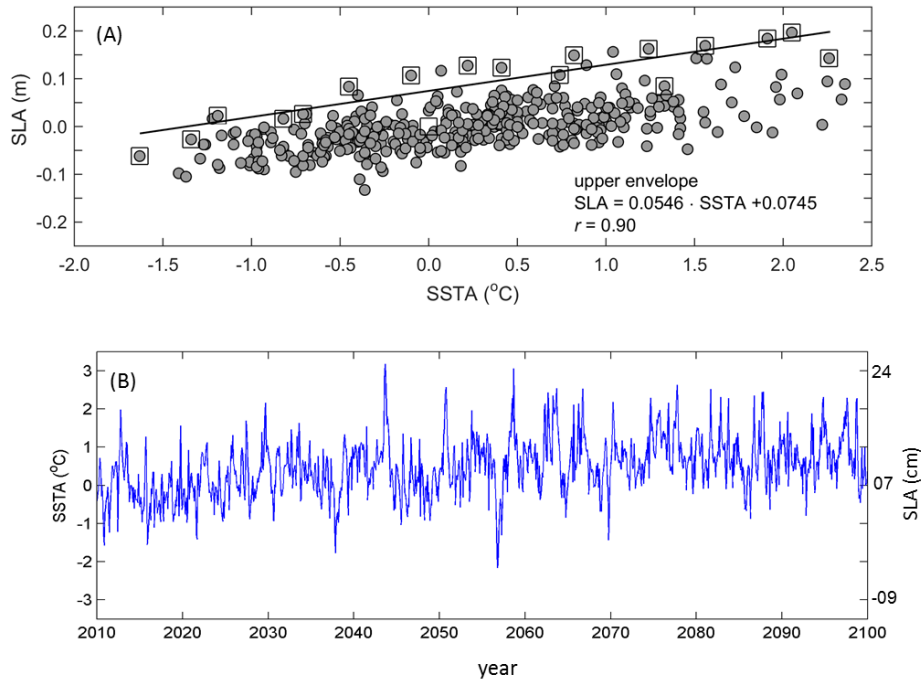


Figure 3. Plots illustrating the empirical relationship and results of sea level anomalies (SLAs) used in model simulations. (A) Linear regression model relating sea surface temperature anomalies (SSTA) and SLAs at La Jolla, CA. Squares highlight the data points of the upper envelope that were used to derive the linear model (solid line). (B) Projected SSTAs (left-hand y-axis) and SLAs (right-hand y-axis).

Atmospheric forcing

Space- and time-varying wind (split into eastward and northward components) and sea level pressure (SLP) fields were applied to all grid cells at each model time-step. The wind and SLP fields were input as equidistant points spaced 10 km apart and interpolated within the Delft3D model to the SWAN and FLOW grids. An average pressure of 101.3 kiloPascals (kPa) was applied to the open boundaries of the meteorological grid.

Winds and SLPs stem from a recently (2015) derived 10 km resolution dataset of hourly winds and sea level pressures. The California Reanalysis Downscaling at 10km (CaRD10) is a reconstruction of the high-spatial resolution / high-temporal scale analysis of atmosphere and land covering the state of California for global change studies (Kanamitsu and Kanamaru, 2007; SIO, 2015). CaRD10 data is generated by dynamically downscaling coarse atmospheric data using Scripps' Experimental Climate Prediction Center Hydrostatic Global to Regional Spectral Model (G-RSM). The downscaling includes scale-selective bias corrections to suppress large scale errors, yet stay true to the large scale forcing fields, and does not use any observations except sea surface temperatures (SSTs) to adjust the results. Two subsections of the CaRD10 database were used for CoSMoS application to the Southern California study region: 1) a hindcast period derived from dynamical downscaling of the National Centers for Environmental Prediction (NCEP) Global Forecast System (GFS) model Global Reanalysis (available years 1975 to 2010 at 32 km, 3 hourly resolution) and 2) a future period (2011 – 2100 at 2.5° x 1.5°, 3 hourly resolution) derived from the same RCP4.5 GFDL-ESM2M GCM used in the global-scale wave downscaling.

Deep water wave forcing

Deep water wave parameters (H_s , T_p , and D_p), obtained with the WW3 model for the CDIP067 buoy were applied along all open boundaries of the Tier I SWAN grid. Alongshore variations in deep water wave forcing available with the WW3 model outputs were small, particularly with respect to incident wave directions, which are critical to accurate computations of wave propagation from deepwater to the SCB nearshore region where sheltering effects are important (Rogers and others 2007).

3.3 Local scale 2D wave and hydrodynamic model – Tier II

Grids, model settings, bathymetry and topography

Tier II consists of 11 local-scale sub-models, each consisting of two SWAN grids and multiple FLOW grids (fig. 4). San Diego and Los Angeles Counties each include three sub-models, Orange and Ventura Counties two sub-models, and Santa Barbara was comprised of one sub-model (Table 2). Physical overlap exists between sub-models along-shore extents in order to avoid erroneous boundary effects in regions of interest.

Each Tier II hydrodynamic FLOW sub-model consists of one ‘outer’ grid and multiple two-way coupled ‘domain decomposition’ (DD) structured grids. DD allows for local grid refinement where higher resolution (~10 m - 50 m) is needed to adequately simulate the physical processes and resolve detailed flow dynamics and overland flood extents. Communication between the grids takes place along internal boundaries where higher-resolution grids are refined by 3 or 5 times that of the connected grid. This DD technique allows for two-way communication between the grids and for simultaneous simulation of multiple domains (parallel computing), reducing total computation time while maintaining high resolution computations.

In the landward direction, Tier II DD FLOW grids extend to the 10 m topographic contour; exceptions exist where channels (e.g., the Los Angeles River) or other low-lying regions reach very far inland. The number of DD FLOW grids ranges from 4 to 13, depending on local geography, bathymetry, and overall setting. Grid resolution ranges from approximately 130 m x 145 m (across and along-shore, respectively) in the offshore region to as fine as 5 m x 15 m in the nearshore and overland regions.

Wave computations are accomplished with the SWAN model using two grids for each Tier II sub-model: one larger grid covering the same area as the ‘outer’ FLOW grid and a second finer-resolution two-way coupled nearshore nested grid. The nearshore SWAN grids extend from at least the 30 m isobath to well inland of the present day shoreline. The landward extension is included to allow for wave computations of the higher SLR scenarios.

All model settings of the Tier II domains are identical to those used for Tier I runs, with the exception of the time-step (10 seconds) and threshold depth (1 cm) in the hydrodynamic FLOW models. The threshold depth is used within the model to assign a grid cell as either wet or dry. For the flooding and drying scheme, the bottom is assumed to be represented as a staircase of tiles centered around the grid cell water level points. If the total water level drops below 1 cm, then the grid cell is set to dry. The grid cell is again set to wet when the water level rises and the total water depth is greater than the threshold.

Table 2. Tier II sub-model extents, number of grids, and grid resolutions.

Sub-model name	Geographic extents* (north to south)	Counties**	Number of DD grids	Grid resolution (m)	
				Most coarse*	Finest
gc	Point Conception to Carpinteria	SB	6	70 x 90	18 x 16
ve	Carpinteria to Oxnard Beach	SB / VE	13	100 x 110	5 x 15
is	Oxnard Beach to Point Mugu	VE	6	90 x 90	5 x 15
pm	Point Mugu to Malibu	VE / LA	8	100 x 110	20 x 20
mk	Malibu to Palos Verdes	LA	4	130 x 145	30 x 40
la	Palos Verdes to Seal Beach	LA / OR	4	90 x 115	25 x 45
oc	Seal Beach to Huntington Bch.	OR	12	7 x 11	35 x 65
np	Huntington Bch to San Clemente	OR	9	70 x 85	5 x 8
cb	San Clemente to Encinitas	OR / SD	9	30 x 60	10 x 15
ty	Encinitas to La Jolla	SD	6	30 x 60	10 x 20
sd	La Jolla to Punta Bandera	SD </td <td>9</td> <td>90 x 140</td> <td>10 x 13</td>	9	90 x 140	10 x 13

* excluding the 'outer' FLOW grid but including grids where XBeach is used for flooding calculations

** SB: Santa Barbara; VE: Ventura; LA: Los Angeles; OR: Orange; SD: San Diego

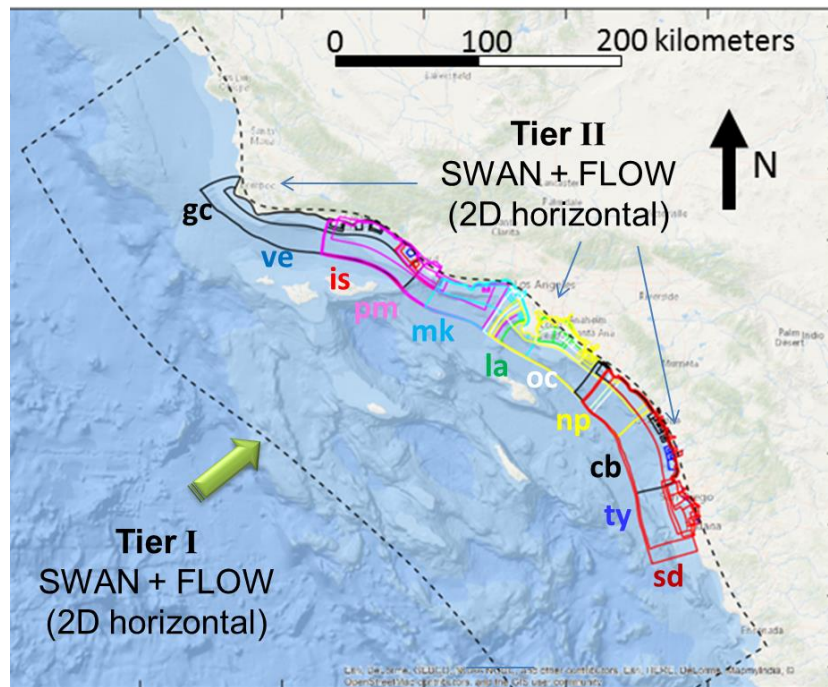


Figure 4. Map showing Tier II model grid extents.

Bathymetry and topography is represented with a seamless digital elevation model (DEM) constructed by the USGS Coastal National Elevation Database (CoNED) team using the most recent, high-resolution topographic and bathymetric datasets available (<http://topotools.cr.usgs.gov/coned/index.php>). Topography is composed of bare-earth data derived from topographic and bathymetric light detection and ranging (Lidar) data and bathymetry from multi- and single-beam sonars. The DEM was constructed to define the shape of nearshore, beach, and cliff surfaces

as accurately as possible, utilizing dozens of bathymetric and topographic data sets. The vast majority of the data was derived from the Coastal California Data Merge Project which includes lidar data collected from 2009 through 2011 and multi-beam bathymetry collected between 1996 and 2011 extending out to the three nautical mile limit of California's state waters (NOAA, 2016; <https://catalog.data.gov/dataset/2013-noaa-coastal-california-topobathy-merge-project>). Harbors and some void areas in the nearshore were filled in with bathymetry from either more recent multi-beam surveys, 1/3 arc-second (~10 m resolution) NOAA coastal relief model data, or single-beam bathymetry. In deeper waters offshore of the three nautical mile limit (~5.6 km) the 10 m resolution NOAA coastal relief models were used (<http://www.ngdc.noaa.gov/dem/squareCellGrid/map>). Following compilation of the topography and bathymetry data, the DEM was 'hydro-enforced' to provide water flow connectivity between open sluices, canals, and under bridges and piers. The final nearshore DEM consists of 2 m resolution data extending from the 20 m isobath to the 20 m elevation contour. These data were used to populate the majority of the Tier II grids and generate initial profiles for the 0 m SLR of the nearly 4,500 cross-shore transects (CSTs) used for Tier III XBeach modeling. A second DEM of 10 m gridded resolution is used to represent deeper water conditions extending seaward of the three nautical mile limit. All data are referenced to the NAD83 and NAVD88 horizontal and vertical datums, respectively, and both Tier II and Tier III models run in projected UTM (zone 11 S) coordinates.

Boundary forcing

Water level and Neumann time-series, extracted from Tier I simulations, were applied to the shore parallel and lateral open boundaries of each Tier II 'sub-model outer' grid, respectively. Several of the sub-models proved to be unstable with lateral Neumann boundaries; for those cases one or both of the lateral boundaries were converted to water level time-series or left unassigned. The open boundary time-series were extracted from completed Tier I simulations so that there is no communication from Tier II to Tier I (i.e. one-way communication).

The water level time-series extracted from Tier I and applied at the open boundaries of the 'nested' sub-models included variations due to tides, SLAs and storm surge, the latter of which is computed with spatial and time-varying winds and SLPs across the continental shelf. In order to account for further contributions of winds and SLPs to storm surge related wind-setup at the shore and local inverse barometer effects (IBE, rise or depression of water levels in response to atmospheric pressure gradients), the same 10 km hourly resolution winds used in Tier I are also applied to each grid cell in the Tier II sub-models.

A set of gauged and ungauged rivers and tributaries considered most relevant in influencing coastal flooding were selected and included in the Tier II sub-models. A total of 41 time-varying fluvial discharges are applied either at the closed boundaries or distributed as point sources across grid cells within the relevant model domains (table 3). See Section 3.6 for explanations of how the time-series were derived.

Table 3. Fluvial discharge points included in Tier II model runs.

River or creek	Longitude (DD)	Latitude (DD)	Tier II sub-model	River or creek	Longitude (DD)	Latitude (DD)	Tier II sub-model
Jalama	-120.49939	34.51268	gc	Los Angeles	-118.18076	33.80757	la, np
Gaviota	-120.23122	34.47670	gc	San Gabriel	-118.07196	33.77822	la
Refugio	-120.06830	34.46742	gc	Bolsa Chica	-118.03087	33.71205	oc
El Capitan	-120.02231	34.46286	gc	Newport Bay	-117.83347	33.66012	np
Goleta3	-119.83536	34.43268	gc	Santa Ana	-117.94888	33.65797	la
Goleta4	-119.81935	34.43188	gc	San Juan	-117.66907	33.45832	sd
Goleta	-119.85164	34.43088	gc	San Mateo	-117.57813	33.38536	cb
Goleta2	-119.85164	34.43088	gc	San Onofre	-117.57183	33.37625	cb
Devereux	-119.86817	34.41682	gc	Santa Margarita	-117.38939	33.23724	cb
Arroyo Burro	-119.74090	34.40523	gc	San Luis Rey	-117.37455	33.20970	cb
Carpinteria SM1	-119.52549	34.40462	gc	Buena Vista	-117.33367	33.18381	cb
Carpinteria SM2	-119.52549	34.40462	gc	Agua Hedionda	-117.30445	33.14778	cb
Rincon	-119.47326	34.37774	gc	Batiquitos	-117.26057	33.09203	cb, ty
Ventura	-119.30830	34.28100	gc, is	San Elijo	-117.25114	33.01976	ty
Santa Clara	-119.25637	34.24017	is, ve	Del Mar	-117.23189	32.97878	ty
Calleguas	-119.08061	34.11838	is	Pensaquitos	-117.20610	32.91575	ty
Mailbu	-118.68000	34.04093	mk, pm	San Diego	-117.19646	32.76264	sd
Mission	-118.08840	34.01668	gc	Sweetwater	-117.05831	32.63631	sd
Ballona	-118.42808	33.97935	mk	Otay	-117.08671	32.59734	sd
Carbon Creek	-124.03430	33.87050	la, np	Tijuana	-117.10233	32.56456	sd
Dominguez	-118.25991	33.81453	la				

Time- and space-varying 2D wave spectra extracted from completed Tier I simulations were applied approximately every km along the open boundaries of the ‘outer’ Tier II sub-model SWAN grids. Space and time-varying wind fields were also applied to both Tier II SWAN grids to allow for computation of local wave generation.

3.4 Local scale 1D wave and hydrodynamic model – Tier III

Grids, model settings, bathymetry and topography

Nearshore hydrodynamics, wave setup, total wave runup and event-based erosion were simulated with the XBeach (eXtreme Beach) version 1.21.3667 (2014) model (Roelvink and others, 2009). XBeach is a morphodynamic storm impact model specifically designed to simulate beach and dune erosion, overwash, and flooding of sandy coasts. XBeach was run in a profile mode, at 4,466 CSTs numbered consecutively from 1 at the U.S. / Mexico border to 4,802, north of Point Conception. Profiles across harbor mouths, inlets, etc. were excluded from the XBeach simulations. Each of the profiles extend from the approximate -15 m isobath to at least 10 m above NAVD88 but are truncated in cases where a lagoon

or other waterway exists on the landward end of the profile. Two meter resolution bathymetry and topography were extracted from the seamless DEM (see section 3.3) along each of the CSTs and resampled to generate a cross shore grid with relatively larger grid cells offshore, hence reducing run times. In simulations with increased SLR, the original profiles were modified to represent long-term morphodynamic change (see section 3.5). Cross shore grid resolution ranged from 5 m onshore and in shallow water depths to between 25 m and 35 m in the offshore, depending on long wave resolution at the offshore boundary, depth to grid size ratio, and grid size smoothness constraints.

Sediment transport was computed in XBEACH with the Soulsby-van Rijn (Soulsby, 1997) transport formula and bore averaged equilibrium sediment concentrations. A median grain diameter of 0.25 mm and sediment thickness of 2 m was assumed for all profile models. Bottom roughness is set to a uniform Chezy value of 65, horizontal background viscosity of 0.01 m²/s, and a flooding and drying threshold depth of 1 cm, similar to Tier II. Initial profile sections of steepness in excess of 32° (angle of repose of natural sand) are assumed to be hard structures or cliffs and set to be immobile (not allowed to erode or accrete during the storm). All simulations are run with a morphological acceleration factor of 10 to speed up the morphological time scale relative to the hydrodynamic timescale and thus reduce computation time.

With regards to wave computations, the XBeach model was run with an instationary wave solver but in a hydrostatic (no vertical pressure gradients) mode, and thus computed hydrodynamics and morphodynamic change associated with wave groups rather than individual waves. Wave breaking and dissipation is modeled after Roelvink (1993) where dissipation is proportional to the wave height to the third order divided by local water depth.

Boundary forcing

Hourly time-series of water levels extracted from completed Tier II runs were applied at the seaward ends (-15 m isobaths) of each of the profile models. These water level variations represented the cumulative effect of astronomic tides, storm surge (including IBE and wind setup), SLAs, and SLR. Neumann boundaries set to zero were used along the lateral boundaries: a condition that has been shown to work well with quasi-stationary situations where the coast can be assumed to be uniform alongshore outside the model domain (Roelvink and others, 2009).

Time series of H_s , T_p , and D_p saved at 20 minute intervals from the nested high resolution Tier II SWAN grid were also applied at the offshore boundary of each profile model. Sensitivity tests comparing the use of these bulk parameters versus full 2-dimensional spectral descriptions output from SWAN showed little difference in the modeled runup, and thus the simpler, and less memory-intensive, approach employed in this study was use of bulk statistical representation of wave conditions as forcing. Bulk parameters extracted from the Tier II simulations were converted to parametric Jonswap spectra by the XBeach model using a 3.3 peak enhancement factor and a cosine law directional spreading coefficient of 10.

3.5 Long-term morphodynamic change models

To better characterize and incorporate the impact of long-term morphologic change on flood hazards, a cliff recession model and a sandy coast shoreline change model were developed for this study (purple trapezoid in fig. 2). Both models are transect based, one-line models, that were used to predict cliff

top recession and lateral movement of the mean high water (MHW) position at the CSTs used to simulate wave setup and runup with the Tier III XBeach model.

The cliff recession model (Limber and others, 2015) employs a suite of models, including 2-D process-based soft rock (loosely consolidated sediment deposits) and hard rock (indurated lithologies such as sandstone or granite) models, and several empirical 1-D models that relate wave impacts and water level variations (e.g. storm surges, sea level anomalies) directly to cliff edge retreat through time (Trenhaile, 2000, 2009, 2011; Walkden and Hall, 2005; Walkden and Dickson, 2008; Hackney and others, 2011; Revell and others, 2011).

The sandy coast shoreline change model (CoSMoS Coastal One-line Assimilated Simulation Tool CoSMoS-COAST; Vitousek and others, 2015) incorporates historical trend analysis and three process-based models that compute both long- and cross-shore transport of sandy shores (Pelnard-Considere, 1956; Bruun 1962; Larson and others, 1997; Davidson-Arnott, 2005; Yates and others, 2009; Long and Plant, 2012; Anderson and others, 2015; Vitousek & Barnard, 2015). Historical shoreline positions and a Kalman filter were used to auto-tune the model parameters (Long and Plant, 2012) and to implicitly account for unresolved sediment transport processes and inputs, such as sediment loading from rivers and streams, regional sediment supply, and long-term erosion.

The cliff and shoreline models were used to project cliff top recession and movement of the MHW line, respectively, for nine SLR scenarios (0.25 m to 2 m, at 0.25 m increments, and 5 m). Projected time-series of SLR and waves (height, period, and incident direction) at the offshore ends of the CSTs served as boundary conditions for both the cliff recession (2,017 profiles) and shoreline change (4,011 profiles) models.

SLR was represented with a second-order polynomial curve that reached 1 m or greater by the year 2100, relative to 2000. For SLR rates of 0.25 m, 0.50 m and 0.75 m, long-term morphodynamic change simulations were run up through Jan 01, 2044, 2069, 2088, respectively, based on the National Research Council (2012) values for Southern California (2012).

Projected wave time-series were derived from a look-up-table constructed from numerical simulations. The look-up-table relates deep-water waves to nearshore wave conditions and was developed from a 30-year hindcast (Hegermiller and others, 2016). Using this look-up-table and dynamically downscaled GFDL-ESM2M RCP4.5 wave projections (see Section 3.1), 100+ year long time-series of 3-hourly nearshore wave conditions were generated at each of the CSTs and used as boundary conditions to the long-term morphodynamic change models (gray trapezoid in fig. 2). This approach of developing and using a look-up-table, was done because of the high computational expense associated with computing long (100+ years) continuous time-series within the large geographic extent of the SCB.

Several different management scenarios involving beach nourishment and the existence and maintenance of hard structures to limit erosion were simulated with both the cliff recession and sandy shoreline change models. Two management scenarios were investigated for the cliff recession projections: (1) cliff recession unlimited by cliff armoring, and (2) no cliff recession where armoring currently (2016) exists. For the sandy shoreline projections, four management scenarios were simulated, representing all combinations of: (1) no beach nourishment or continued rates of historical beach nourishment were investigated for the sandy shoreline simulations, and (2) the existence or non-existence of hard structures that limit erosion. This “hold-the-line” hard-structures scenario was achieved by limiting erosion to an 180,000-point polyline digitized from aerial photos (Google Earth, 2015/2016) that represents the division of beach and urban infrastructure.

Feedback between the cliff and shoreline change models was not incorporated for this application. However, the cliff recession model did include foreshore accretion in cases of failed cliff material. In future model applications, the CoSMoS-COAST and cliff retreat models will be coupled together. Incorporating long-term morphodynamic change with the flood modeling

Incorporating long-term morphodynamic change with the flood modeling in CoSMoS 3.0 Phase 2, was done by evolving the original (0 m SLR) cross-shore profiles by the projected long-term cliff recession and MHW positions associated with each SLR. The selected long-term management scenario assumed that beach nourishment would cease but that existing cliff armoring and flood/beach protection infrastructure remains in place (i.e., the “hold-the-line” scenario). The resulting ‘evolved’ profiles were then used to simulate inundation and runup with the Tier III XBeach model (Section 3.4). No adjustments were made to the depth and topography representations in the Tier II Delft3D high-resolution grids that were used to simulate inland flooding (Section 3.3).

Profile changes incorporated recession of the cliff top and consequential retreat of the cliff face, lateral migration of the MHW position, and vertical translation in keeping with SLR (fig. 5). These shoreline modifications were made only within the active beach region and up to the urban development boundary used to “hold-the-line”.

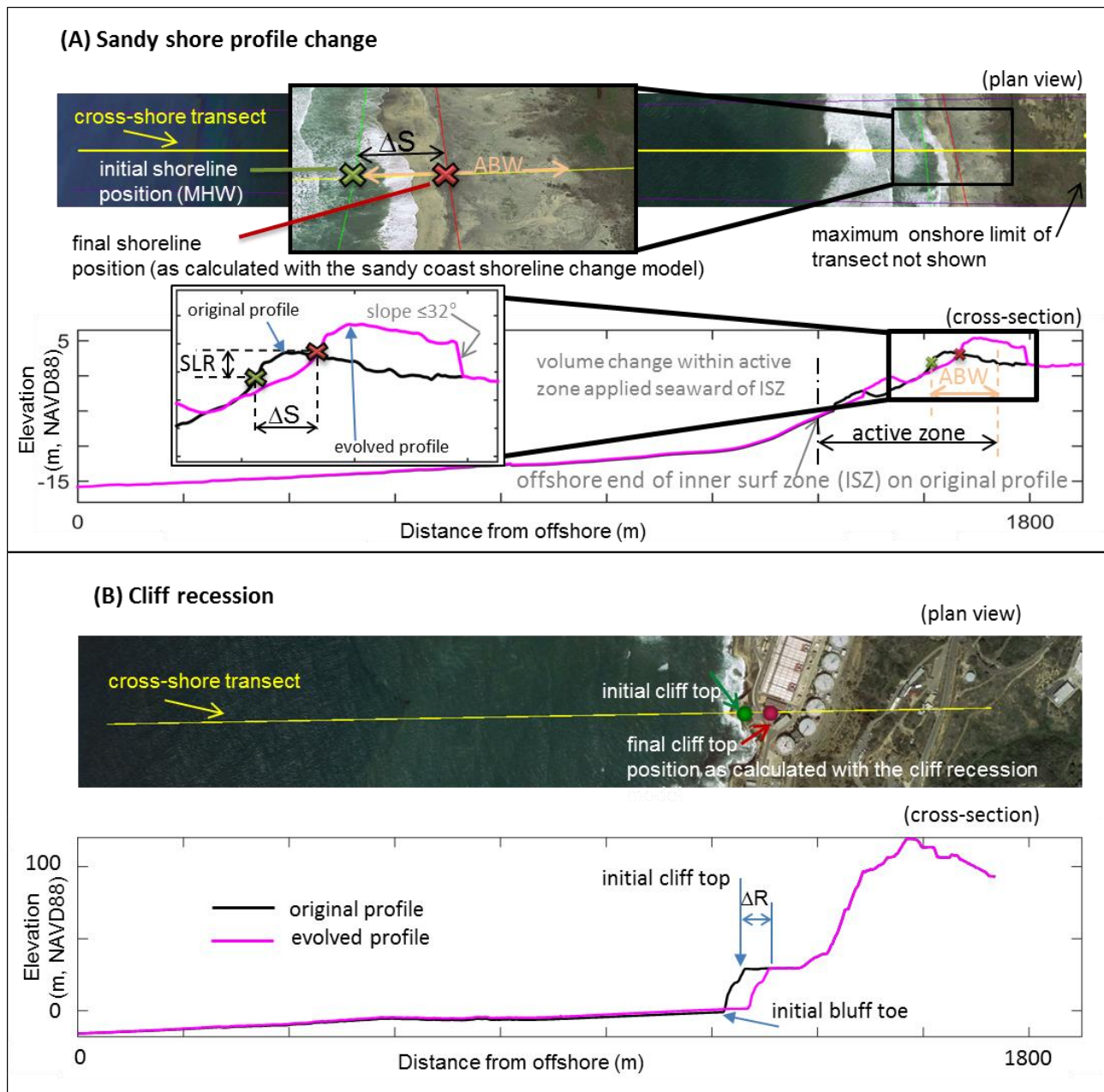


Figure 5. Example profile types considered in merging cliff and shoreline model projections. (A) Schematic of key parameters used in the evolution of soft (sand and gravel) beaches (ΔS : = change in mean-high-water position; ABW: active beach width). (B) Schematic of key parameters used in the evolution of cliff profiles (ΔR : = cliff recession).

3.6 Fluvial discharge model

At the time of this study, there were no available time-series of 21st century discharge rates associated with the RCP 4.5 scenario, and therefore idealized hydrographs were constructed. Idealized hydrographs were generated by parameterization of peak discharge rates and estimation of the duration and rate of increase and decrease of discharges associated with coastal storm events.

Peak discharge rates

Fluvial discharge points considered most relevant in influencing coastal flooding and used within the Tier II model domains were separated into two groups: 1) gauged streams and rivers for which we were able to identify a relationship between peak flows and an independent atmospheric variable available as part of GCM model outputs (which after testing turns out to be SLP gradients, ∇SLP), and 2) subordinate rivers and tributaries. Variants of SLPs, a readily available parameter in GCM outputs, were tested against peak discharge rates measured at 18 USGS gauging sites. Peak discharge rates were defined as the 99.95th percentile flow rate from records that were at least 40 years long and sampled at 15 minute intervals (<http://waterdata.usgs.gov/ca/nwis/rt>). Reasonably strong linear relationships ($0.42 < r < 0.92$, p -values between 0.003 and 0.731) were found between maximum sea level pressure gradients (∇SLP) and peak discharge at 7 stations (table 4). ∇SLP were computed with the CaRD10 hindcast covering 3 days prior to peak discharge and within a 0.67° to 1° radius of the gauging station. Time periods within 1, 3, and 5 days preceding an event and within 0.67° , 1° , and 5° search radii were tested. Best fits were obtained with the 3 day window and 0.67° search radius for all sites but Santa Ana and Santa Margarita for which a 1° search radius gave the best results. Whereas the correlation for Ventura and Santa Margarita Rivers were somewhat poor (correlation coefficients, $r = 0.49$ and $r = 0.42$, respectively, see table 4) these discharge points were kept because of the lack of alternative major surrogate rivers in these locations.

The linear relationship established between measured peak fluvial discharge rates and ∇SLP allows for an estimate of peak discharge events associated with future storms. In CoSMoS, ∇SLP were calculated for each primary discharge site from GCM pressure fields associated with a particular storm. These values were used in the linear model with appropriate coefficients (last columns in table 4) to estimate peak discharge rates (in m^3/s) for a given storm.

Table 4. Primary fluvial discharges: gauged stations for which linear relationships between fluvial discharge (Q) and sea level pressure gradients (∇SLP) were established.

USGS gauging station ID	station name	Drainage area (km^2)	r	p -val	best fits $Q=m\cdot\nabla\text{SLP}+b$	
					m	b
11119750	Mission Ck	22	0.82	0.022	1.577E-07	2.234E-07
11120000	Atascadero	49	0.92	0.003	2.060E-07	-4.621E-08
11118500	Ventura River	487	0.48	0.274	1.503E-07	-2.131E-07
11106550	Calleguas Creek	642	0.74	0.058	6.303E-08	-1.909E-08
11102300	Rio Hondo (L.A. trib.)	321	0.78	0.040	7.094E-08	1.376E-06
11078000	Santa Ana	4403	0.66	0.103	1.662E-08	-2.358E-08
11046000	Santa Margarita	1873	0.42	0.731	2.702E-08	-1.208E-08

Sub-ordinate rivers and tributaries were assigned to one of the nine primary discharges (table 5; fig. 6) based on proximity and location relative to the primary watersheds as well as previous studies that have evaluated similar relationships (Warrick and Farnsworth, 2009). Peak discharge rates associated with individual storm events were estimated by assuming that the runoff rates of the subordinate discharges,

defined as the fluvial discharge rate divided by the drainage area, are equal to the runoff rate of the primary discharge (see flow chart in fig. 6). Drainage areas upstream of each gauging station were derived from USGS 12-digit and 8-digit (where necessary) watershed boundaries, local water district maps (for verification and inclusion of all necessary tributaries), and other published sources.

Table 5. Sub-ordinate rivers and tributaries, drainage areas, and associated primary discharges.

Sub-ordinate river/tributary	Drainage area (km²)	USGS gauging station	Sub-ordinate river/tributary	Drainage area (km²)	USGS gauging station
Primary discharge: Atascadero			Primary discharge: Santa Margarita		
Jalama	64	11120000	San Juan	303	11046000
Gaviota	52	11120000	San Mateo	346	11046000
Refugio	21	11120000	San Onofre	111	11046000
El Capitan	16	11120000	Los Flores	69	11046000
Devereux	10	11120000	Santa Margarita R	1,916	11046000
Goleta	15	11120000	San Luis Rey	1,442	11046000
Goleta2	15	11120000	Buena Vista	56	11046000
Goleta3	15	11120000	Agua Hedionda	77	11046000
Goleta4	24	11120000	Batiquitos	138	11046000
Goleta5	51	11120000	San Elijo	219	11046000
Primary discharge: Mission Creek			Del Mar	894	11046000
Arroyo burro	25	11119750	Pensaquitos	244	11046000
Mission	30	11119750	San Diego	976	11046000
Carp_SM1	1	11119750	Sweetwater	564	11046000
Carp_SM2	7	11119750	Otay	367	11046000
Rincon	38	11119750	Tijuana	4,390	11046000
Primary discharge: Ventura			Primary discharge: Rio Hondo		
Ventura R	487	11118500	Ballona	332	11102300
Santa Clara R	4,128	11118500	Dominguez	175	11102300
Primary discharge: Calleguas			Bolsa Chica	5	11102300
Mailbu	284	11106550	Newport Bay	306	11102300
			Primary discharge: Santa Ana		
			Los Angeles R	2,156	11078000
			San Gabriel R	1,658	11078000

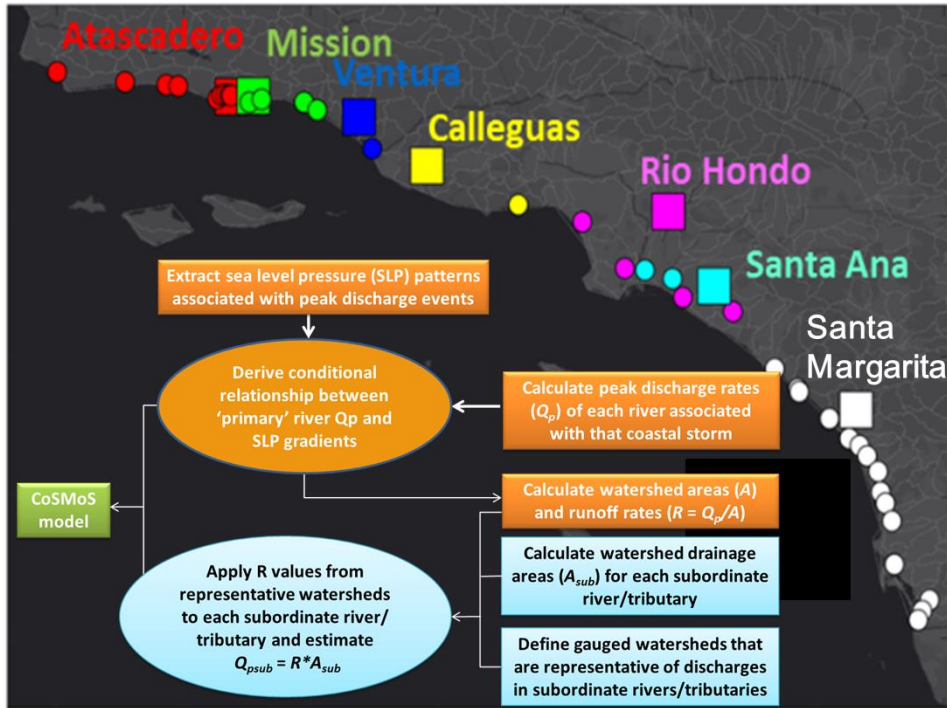


Figure 6. Schematic of approach used to estimate peak fluvial discharge rates associated with atmospheric storm patterns for coastal storms simulated with CoSMoS ver. 3.0. Primary discharges and sub-ordinate rivers and tributaries are color coded in the map figure. The flow chart details the method used to derive a conditional relationship between atmospheric storm patterns and peak fluvial discharge rates of ‘primary discharges’ (filled squares) and the method used to derive peak flows of sub-ordinate discharges (filled circles).

Idealized hydrograph

An idealized hydrograph was developed with the aim of estimating the duration and rate of increase and decrease of peak discharge events. Stations where data were available at 15 minutes or better sampling resolution, and for which at least 4 events exceeded the 99.95th percentile during the record period, were used to develop the hydrograph. Nine stations within the study area met these criteria (table 6). Events that exceeded the 99.95th percentile (column 7 in table 6) were selected, normalized, and used to develop the hydrograph assuming a lognormal distribution. The shape of the idealized hydrograph is skewed toward rapid initial increases in flow and subsequent slower rates of decreasing discharge rates (fig. 7). The total duration is on the order of 0.7 days (17 hours) for flows that exceed 10% of the peak discharge.

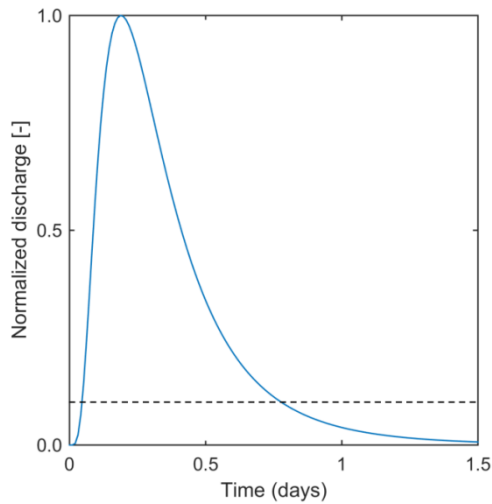


Figure 7. Idealized hydrograph. Dashed horizontal line indicates 10% peak discharge rates.

Table 6. Gauging stations and details of each for development of unit hydrograph.

USGS gauging station ID	Lat (°N) (NAD27)	Lon (°E) (NAD27)	Length of record (years)	Mean flow (m ³ /s)	Median flow (m ³ /s)	99.95th percentile (m ³ /s)	# events ≥99.95th percentile	Lognormal mean (days)	Lognormal variance (days)	
11119750	34.428	-119.725	44	0.06	0.00	13	5	-1.51	0.84	
11120000	34.425	-119.812	73	0.14	0.00	38	5	-3.66	1.80	
11109000	34.404	-118.739	87	1.67	1.08	77	5	-1.11	0.80	
11119500	34.401	-119.487	74	0.05	0.00	14	4	-1.30	0.79	
11106550	34.179	-119.040	46	0.97	0.31	120	3	-1.48	0.90	
11092450	34.162	-118.467	83	2.90	1.84	290	6	-2.12	1.51	
11048600	33.645	-117.861	14	0.05	0.02	9	8	-3.27	1.46	
11047300	33.498	-117.666	42	0.45	0.08	61	5	-3.10	1.42	
11046000	33.311	-117.347	92	0.89	0.13	98	5	-2.15	1.01	
			mean	61.73	0.80	0.38	80	5	-2.19	1.17
			min.	13.51	0.05	0.00	9	3	-3.66	0.79
			max.	91.89	2.90	1.84	290	8	-1.11	1.80

Section 4. Identification of storm events

The model system, which aims to account for the most relevant atmospheric and oceanic processes that might contribute to future flooding and associated coastal hazards and the inter-related non-linear physics of each of these, requires downscaling from the global to local level and is computationally expensive. Because of the long simulation times, it is not feasible to run all Tiers for the entire 21st century time-

period. Instead, a hybrid numerical-analytical downscaling approach was developed to estimate total water levels (TWL), inclusive of storm-wave and surge impacts and long-term climatic variation, in the SCB nearshore region. From this, relevant return period storm events were selected and used for Tiers I through III detailed modeling.

TWL time-series up through the year 2100 were computed at 4,802 coastal points within the SCB using downscaled waves (Hegermiller and others, 2016) and SLPs and SSTs from the GFDL-ESM2M RCP 4.5 GCM. The 1-year, 20-year, and 100-year future coastal storm events were identified at each location and clustered with a *k*-means algorithm to delineate coastal segments where individual storms result in similar return period water levels. Clustering of extreme events showed that the more severe but rare coastal flood events (e.g., the 100-year event) occur for most of the region from the same storm. In contrast, different storms from varying directions were responsible for the less severe, but more frequent, local coastal flood events. To this end, two 100-year storms were identified (February 2044 and March 2059), two 20-year storms (February 2025 and February 2095), and three 1-year storms (March 2020, December 2056, and January 2097). Upon completion of 1-year storm simulations using the entire train of models (resolving detailed flow dynamics and wave-current interaction) for a range of SLRs, results showed a single 1-year storm (March 2020) consistently yielded the highest water levels throughout the SCB; thus, Phase 2 1-year projections use contributions from only that storm. Deep water waves, SLAs, and maximum and minimum wind speeds and SLPs within the entire model domain, are summarized for each of the identified storm events in table 7.

Table 7. Boundary conditions associated with each modeled scenario. Deep water wave conditions (Hs, Tp, and Dp) applied at all open boundaries of the Tier I wave grid. Sea level anomalies (SLA) applied uniformly to all model domains. Sea level pressures (SLPs) and wind speeds vary in time and space. Those shown are the minimum and maximum values, respectively, attained somewhere within Southern California Bight domain.

Scenario	Hs (m)	Tp (s)	Dp (degrees)	SLA (m)	Minimum	Maximum
					SLP (kPa)	wind speed (m/s)
background	1.75	12	286	0	NA	NA
1-year storm #1	4.39	16	284	0.16	100.56	22.8
20-year storm#1	5.86	18	281	0.18	100.79	22.3
20-year storm#2	6.13	18	292	0.24	100.41	28.7
100-year storm#1	6.20	16	264	0.19	100.43	26.6
100-year storm#2	6.80	18	287	0.23	98.67	30.3

NA: not applicable

Section 5. Scenarios and Timing of Events

Individual coastal storm events, as represented by high waves, strong winds, low sea level pressures, and large scale phenomenon that produce month long changes in water levels, were modeled in conjunction with a spring tide and various states of sea level rise to simulate the impacts of a ‘scenario’. In CoSMoS version 3.0, each storm is represented by dynamically downscaled waves, winds, and sea-level pressures from the same GCM model, resulting in realistic representations of passing storm systems and internally consistent timing of these processes. However, because storm events and astronomic tides are independent phenomena, a given storm event can occur during any part of the tide cycle. A storm that occurs during high tide may result in substantial flooding and damage, but conversely may impart very

little destruction if the storm were to occur during low tide. For less computationally intensive modeling systems, a probabilistic approach can be taken to evaluate coastal impacts from storms that occur during different stages of the tide, but with the deterministic process-based CoSMoS model that aims to resolve details and non-linear processes, this is not presently feasible. Instead, it is assumed that each storm coincides with a high spring tide (tide levels that occur approximately twice every month for a total of ~8 days). This represents a near-worst case scenario, with the ‘King Tide’ being slightly higher but much less frequent, occurring typically only during two ~3-4 day time periods per year.

Each scenario is simulated over a 24 hour time-period with Tiers II and III (fig. 8). Tier I is run for 28 days to allow for model ‘spin-up’. Sea-level rise and SLA are held constant and uniform through the duration of the scenario. Deep water wave forcing are also held constant throughout the simulation at the open boundary of Tier I, but consequently vary in height and direction as they approach the shore in response to changes in both bathymetry and water levels. SLP fields are shifted in time so that the lowest pressure anywhere within the Tier I model domain aligns in time with the high tide at the Los Angeles tide station (approximate center of the study area, hour 17 in fig. 8), thus “synching” the storm arrival with the high tide level. The wind fields are similarly time-shifted since these are physically linked to the pressures and share a common time-stamp. For fluvial discharges, the peak of the hydrograph is placed 1 hour following the high tide. The timing of the hydrograph was selected based on comparisons between peak fluvial discharge rates at gauging stations close to shore (e.g. Malibu) and hindcast time-series of nearshore wave conditions. Comparisons of these time-series revealed that the peak storm H_s consistently preceded the peak in fluvial discharge rates due to the lag in response time of the associated watersheds.

Forcing / boundary	Timing
tides	varies spatially and temporally and is identical for each scenario
SLR	constant for duration of scenario (but differs between scenarios)
SLA	constant for duration of scenario (but differs between scenarios)
deep water waves	constant for duration of scenario (but differs between scenarios)
SLPs	varies spatially and temporally, timing assigned such that the lowest SLP anywhere within the SoCal Bight aligns with high tide
winds	varies spatially and temporally linked to the timing of SLPs
river discharge	varies temporally at each established USGS gauging site via a idealized hydrograph and derived peak discharge rate based on SLP gradients; timing is hardwired to occur with peak 1hr after high tide

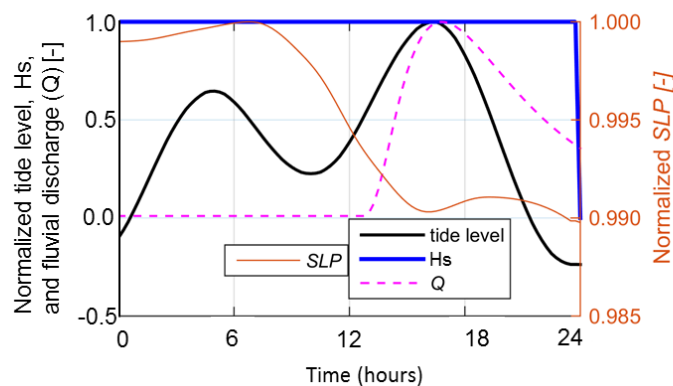


Figure 8. Summary list and plot illustrating timing of individual forcing agents used in model simulations. Abbreviations: SLR: sea-level rise; SLA: sea level anomalies; SLPs: sea-level pressure.

Section 6. Determination of flood extents and uncertainty estimates

Flood extents were determined in two ways: 1) from the landward-most wet grid cell in the high-resolution Delft3D grids, and 2) from maximum wave setup calculated with XBeach cross-shore models along the open coast. Wave setup is the increase in mean water level above the still water line due to the transfer of momentum by waves that are breaking or otherwise dissipating their energy. Wave setup can last from several to ten or more times the length of the incident wave period. Storm-related T_p in southern California are typically on the order of 14 s (CDIP092 for two storm events: Dec 2005 and Jan 2010 storm events); assuming 5 times the dominant incident period of 14s means setup lasts a little less than a minute ($3 \cdot 14$ s) to nearly 5 minutes ($20 \cdot 14$ s). With this in mind, a two minute 8th order Butterworth low-pass filter is applied to water level time-series computed with the XBeach model at the position of the present day MHHW line (1.57 m to 1.63 m above NAVD88). The intersection between the maximum 2-minute sustained water level and landward position of the eroded XBeach profile is then identified and set as the maximum flood extent (fig. 9). Note that except where overtopping occurs or at a narrow beach that fronts a near vertical cliff or wall, this method results in a flood extent that is seaward of the maximum runup in most areas. Maximum runup is also output as part of the CoSMoS results, but are mapped as single points rather than included in the flood extent. This is because runup levels are of shorter duration, and depending on the beach slope, may only constitute a couple of centimeters of intermittent standing water. The event-based erosion extent is dependent on the runup extent.

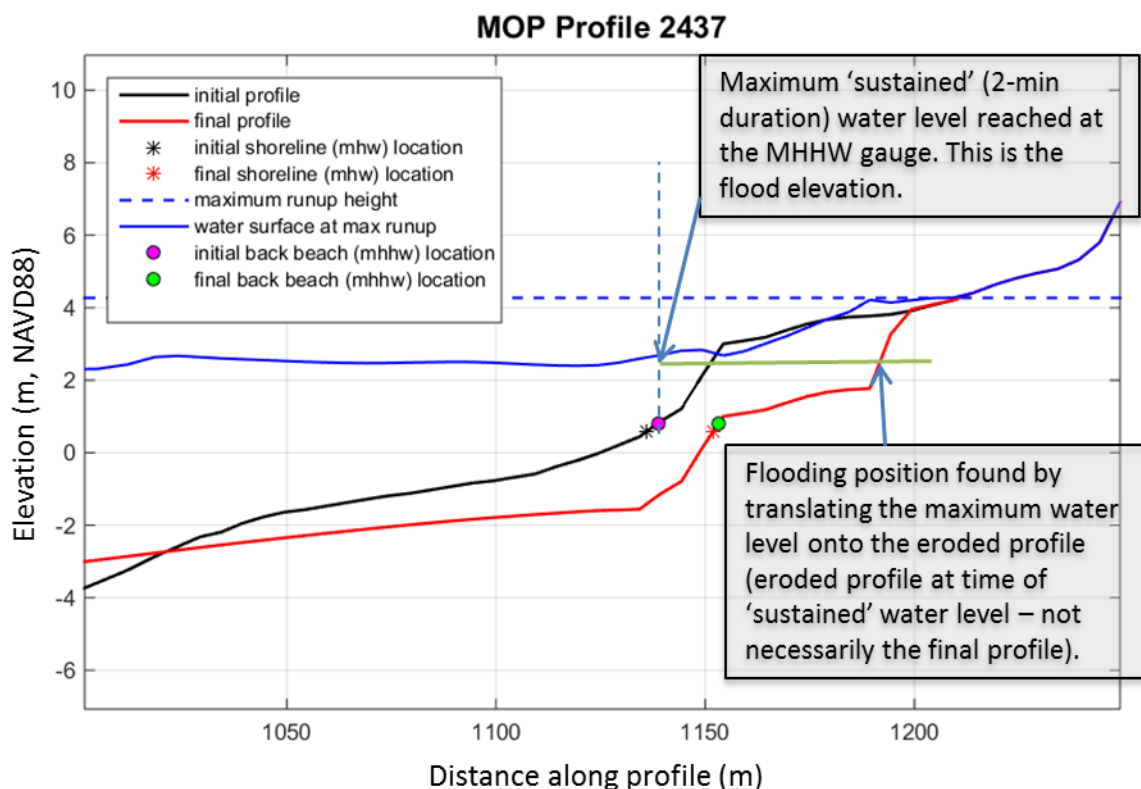


Figure 9. Illustration of method used to determine the flood extent at XBeach cross-shore profile models.

Melding of flood extents simulated with the XBeach and Delft3D high resolution models was done by interpolating (linear Delaunay Triangulation) resulting water level elevations onto a common 2 m resolution square mesh (within the Mathworks Matlab environment). In some areas, such as Mission Beach in San Diego County, where both XBeach and high resolution grids exist to capture flooding from either or both the landward or seaward side, XBeach results were given precedence (fig. 10).

This post-processing step was done for all storms simulated as part of a given scenario. For the 20-year storm for example, two individual storm events were modeled in order to ensure that local effects, such as shoreline orientation with respect to incident storm direction, were taken into account. For those cases where more than one storm was modeled, all resulting 2 m gridded flood maps were overlain and maximum water levels saved at each grid cell to generate a single, composite flood map for a given scenario (fig. 11).

Resulting water elevation surfaces were differenced from the high resolution DEM to isolate areas where the water level exceeds topographic elevations, indicating flooding. For scenarios that include SLR, 2 m DEMs that incorporate long-term morphodynamic changes were used. These DEMs were constructed by replacing original DEM data within the active beach zone with results of the long-term morphodynamic models (Section 3.5). The active beach zone was populated with data from the evolved >4,000 CSTs and additionally with data from sub-profiles spaced ~10 m apart in between the primary CSTs. Shoreline and cliff profile changes of the primary CSTs were projected onto 2 m cross-shore resolution sub-profiles; all CST and sub-CST data (Easting, Northing, elevation(ΔZ)) were then spatially interpolated within the active beach zone of the original DEM, to portray total morphological change.

The resulting flood maps were then processed to exclude isolated wetted areas not hydraulically connected to the ocean; these disconnected areas were flagged as low-lying vulnerable areas below the flood elevation.

Maps of associated maximum flood durations, velocities, and wave heights were processed in a similar manner to that of the flood depths and extents in that they were gridded onto a common 2 m mesh and then combined as illustrated in figure 10. Data that fell outside the flood map extents were removed so that the foot prints of all maps are identical.

Uncertainty bands of the final flood extents take into account numerical model errors, DEM uncertainty, and vertical land motion (VLM). Overall, tidal amplitudes, water levels, wave heights, and wave setup are reasonably well represented by the numerical models (data and comparisons are out of the scope in this document but will be provided in upcoming publications). The area and number of storms tested are however, small in relation to the large geographic scope and thus model error is estimated to be ± 0.50 m. The vertical accuracy of the baseline DEM is estimated to be ± 0.18 m, the 95% confidence level for topographic lidar measurements in open terrain (Dewberry, 2012). Spatially variable measurements of vertical land motion attributed to tectonic movement of the San Andreas Fault System from Howell and others (2016) were also incorporated. Maximum rates of uplift (0.4mm/yr) and subsidence (0.6mm/yr) within our study area equate to a maximum of 3.4 cm of uplift and 5.2 cm of subsidence for the 1m SLR scenario based on the National Research Council (2012) SLR projections for Southern California (2012) of 1m of SLR by the year 2100. The VLM uncertainty for the 1m SLR scenario was also applied for scenarios > 1 m. Uncertainty bands were applied to the final flood maps by raising and lowering the evolved DEMs (or baseline DEM for 0 SLR scenarios) by ± 0.68 m plus elevation uplift or subsidence resulting from VLM. The flood extent uncertainty bands do not take into account additional uncertainty resulting from cliff recession and shoreline change projections in the evolved DEMs. Uncertainties in cliff retreat and shoreline change projections are provided within their respective data files.

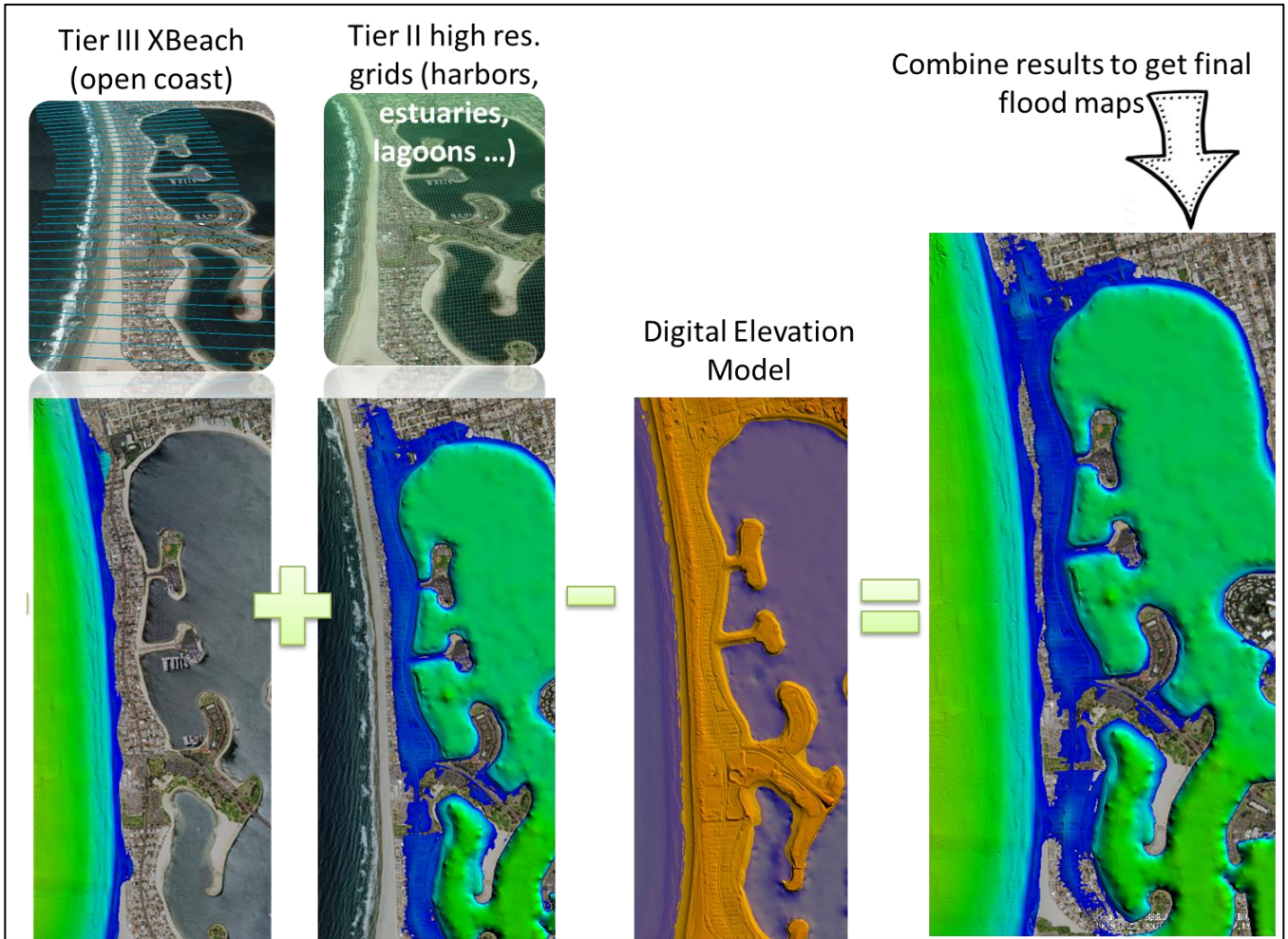


Figure 10. Schematic illustrating melding of Tier II and Tier III flood elevations and extents. Example shown is of Mission Beach, San Diego County.

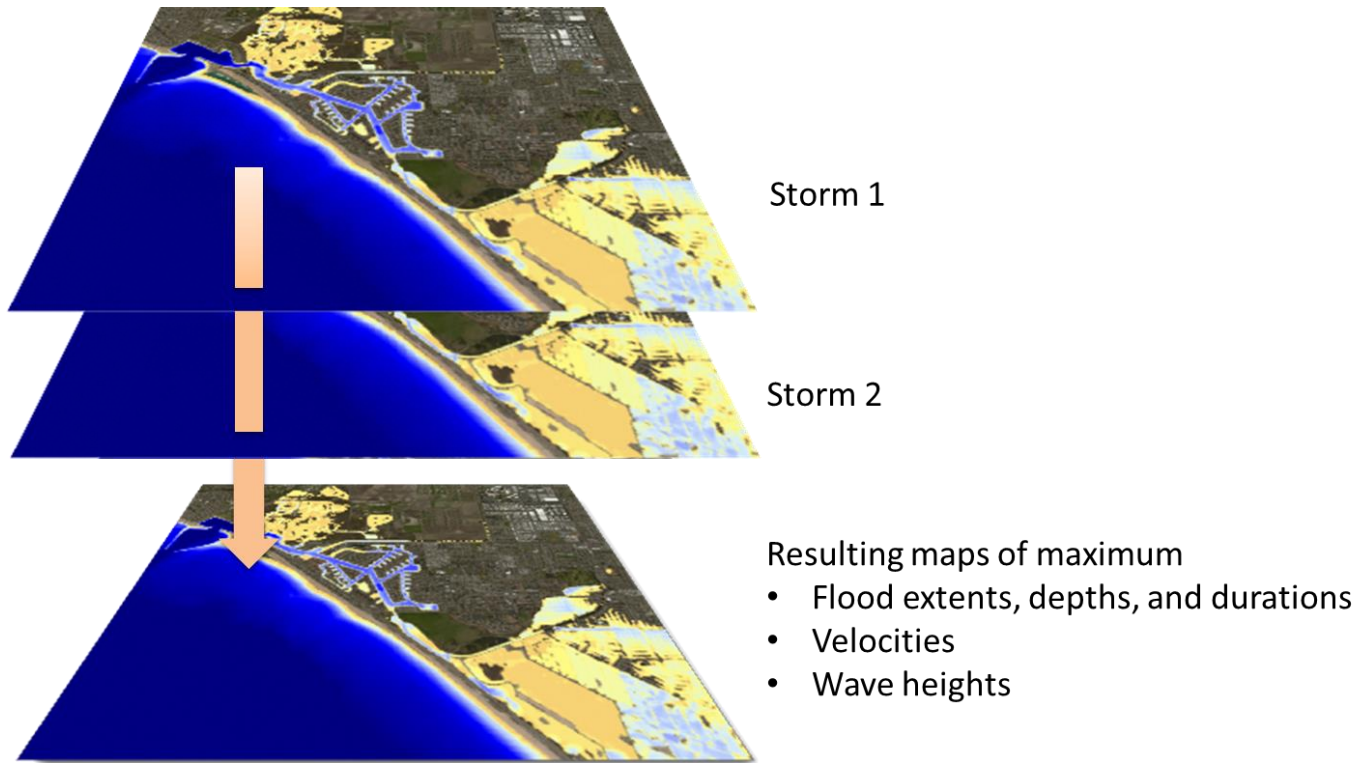


Figure 11. Schematic illustrating the combination of multiple model results from several storm simulations to attain one single map of local maximum values.

Acknowledgements

This work was funded by the USGS Coastal and Marine Geology Program and carried out under the USGS Climate Change Impacts to the U.S. Pacific and Arctic Coasts Project. The initial funding for CoSMoS 3.0, primarily from the California State Coastal Conservancy with additional support from the City of Imperial Beach, California Department of Fish & Wildlife, and Tijuana River National Estuarine Research Reserve (TJNERR), and substantial support from within USGS, was for the preliminary construction of CoSMoS 3.0, including shoreline and cliff model development and the delivery of 5 SLR scenarios (i.e., 0, 50, 100, 150 and 200 cm) in combination with the 100-year coastal storm. Here we report on the data and methods utilized in the continuation of this effort, Phase 2. Phase 2, to include all 40 storm (no storm, annual, 20-year and 100-year) and SLR scenarios (0-2 m in 25 cm increments, plus 5 m) is funded by California's 4th Climate Assessment.

References

- Adams, P. N., Inman, D.L., and Lovering, J.L., 2011. Effects of climate change and wave direction on longshore sediment transport patterns in Southern California. *Climatic Change*, 103,, S211-S228.
- Anderson, T. R., Fletcher, C. H., Barbee, M. M., Frazer, L. N., and Romine, B. M., 2015. Doubling of coastal erosion under rising sea level by mid-century in Hawaii. *Natural Hazards*, 78(1), 75-103.
- Barnard, P.L., van Ormondt, M., Erikson, L.H., Eshleman, J., Hapke, C., Ruggiero, P., Adams, P.N. and Foxgrover, A.C., 2014. Development of the Coastal Storm Modeling System (CoSMoS) for predicting

- the impact of storms on high-energy, active-margin coasts. *Natural Hazards*, Volume 74 (2), p. 1095-1125, <http://dx.doi.org/10.1007/s11069-014-1236-y>
- Booij, N., Ris, R.C., and Holthuijsen, L.H., 1999. A third generation model for coastal regions, Part I – Model description and validation. *Journal of Geophysical Research*, 104(C4), 7649-7666
- Bromirski, P.D., Flick, R.E., and Cayan, D.R., 2003. Storminess variability along the California coast: 1858–2000, *Journal of Climate*, 16(6), 982–993.
- Bruun, P., 1962. Sea-level rise as a cause of shore erosion, *Proceedings of the American Society of Civil Engineers, Journal of the Waterways and Harbors Division*, 88, 117 – 130.
- Cayan, D.R., Bromirski, P.D., Hayhoe, K., Tyree, M., Dettinger, M.D., Flick, R.E., 2008. Climate change projections of sea level extremes along the California coast. *Climate Change*, S57-S73.
- Christiansen R.L., Yeats, R.S., 1992. Post-Laramide geology of the U.S. Cordilleran region. In: Burchfiel BC, Lipman PW, and Zoback ML (eds), *The Cordilleran orogen: conterminous U.S.: the geology of North America [DNAG] Vol. G-3: geological society of America*, 261–406 .
- Crosby, S.C., O'Reilly, W.C., and Guza, R.T., 2016. Modeling long period swell in southern California: practical boundary conditions from buoy observations and global wave model predictions. *J. Atm. Ocean Technology*, in press.
- Davidson-Arnott, R. G., 2005. Conceptual Model of the Effects of Sea Level Rise on Sandy Coasts, *J. of Coastal Res.*, 21, 6, 1116-1172.
- Dewberry, 2012. LiDAR Quality Assurance (QA) Report California, LiDAR and Imagery QA submitted to: NOAA Coastal Services Center, https://coast.noaa.gov/htdata/lidar1_z/geoid12a/data/1124/supplemental/ca2009_2011_ca_coastal_conservancy_m1124_qareport.pdf
- Donat, M.G., Leckebusch, G.C., Wild, S., and Ulbrich, U., 2010. Benefits and limitations of regional multi-model ensembles for storm loss estimations: *Climate Research*, v. 44, p. 211–225.
- Dunne, J.P., John, J.G., Adcroft, A.J., Griffies, S.M.m Hallberg, R.W., Shevliakova, E., Stouffer. R.J., Cooke, W., Dunne, K.A., Harrison, M.J., Krasting, J.P., Malyshev, S.L., Milly, P.C.D., Phillipps, P.J., Sentman, L.T., Samuels, B.L., Spelman, M.J., Winton, M., Winttenberg, A.T., and Zadeh, N., 2012. GFDL's ESM2M global coupled climate-carbon earth system models. Part I: physical formulation and baseline simulation characteristics, *Journal of Climate*, 25, 6646-6665.
- Flick, R. E., 1998. Comparison of California tides, storm surges, and mean sea level during the El Niño winters of 1982–1983 and 1997–1998. *Shore & Beach* 66(3):7–11.
- Egbert, G., Bennet, A., Foreman, M., 1994. TOPEX/POSEIDON tides estimated using a global inverse model. *Journal of Geophysical Research* 99 (C12), 821–824.
- Erikson, L.H., Hegermiller, C.A., Barnard, P.L., Ruggiero, P. and van Ormondt, M., 2015. Projected wave conditions in the Eastern North Pacific under the influence of two CMIP5 climate scenarios. *Journal of Ocean Modelling*, (0000)1-15, <http://dx.doi.org/10.1016/j.ocemod.2015.07.004>
- Cayan, D., Kalansky, J., Iacobells, S., Pierce, D., Franco, G., Anderson, J., Wilhelm, S., Bedsworth, L., Anderson, M., 2016. Sea level rise scenarios for California's fourth climate assessment. Early release, subject to revision.
- Hackney, C., Darby, S. E., & Leyland, J., 2013. Modelling the response of soft cliffs to climate change: A statistical, process-response model using accumulated excess energy. *Geomorphology*, 187, 108-121.

- Hasselmann, S., Hasselmann, K., Allender, J. H., Barnett, T. P., 1985. Computations and parameterizations of the nonlinear energy transfer in a gravity-wave spectrum. Part II: parameterizations of the nonlinear energy transfer for application in wave models, *J. Physical Oceanography*, 15, 1378–1391.
- Hegermiller, C.E., Erikson, L.H., and Barnard, P.L., 2016. Nearshore waves in the Southern California Bight: A 30-year hindcast and 90-year projected time series for the 21st century. U.S. Geological Survey summary of methods to accompany data release.
- Hibbard, K. A., G. A. Meehl, P. Cox, and Friedlingstein, P., 2007. A strategy for climate change stabilization experiments. *Eos, Trans. Amer. Geophys. Union*, 88, doi:10.1029/2007EO200002.
- Howell, S., Smith-Konter, B., Frazer, N., Tong, X., and D. Sandwell. 2016. The vertical fingerprint of earthquake cycle loading in southern California. *Nature Geoscience*, 9, 611–614. <http://dx.doi.org/10.1038/ngeo2741>
- Kanamaru H., and Kanamitsu, M., 2007. Fifty-seven-year California reanalysis downscaling at 10 km (card10). Part ii: comparison with North American regional reanalysis. *J. Climate*, 20, 5572–5592.
- Larson, M., Hansen, H. and N. C. Kraus, 1997. Analytical solution of one-line model for shoreline change near coastal structures, *Journal of Waterway, Port, Coastal, and Ocean Engineering* 123 (4):180-191.
- Lesser, G., Roelvink, J., Van Kester, J., Stelling, G., 2004. Development and validation of a three-dimensional morphological model. *Coastal Engineering*, 51, 883–915.
- Limber, P., Barnard, P.L. and Hapke., C., 2015. Towards projecting the retreat of California’s coastal cliffs during the 21st Century. In: P. Wang, J.D. Rosati and J. Cheng (Eds.), *The Proceedings of the Coastal Sediments 2015*, World Scientific, 14 pp., doi:10.1142/9789814689977_0245
- Long, J. W. and Plant, N. G., 2012. Extended Kalman Filter framework for forecasting shoreline evolution, *Geophys. Res. Lett.*, 39, L13603, doi:10.1029/2012GL052180.
- Meinshausen, M., and Coauthors, 2011. The RCP greenhouse gas concentrations and their extensions from 1765 to 2300. *Climate Change*, 109, 213-241.
- Moss, R. H., and Coauthors, 2010: The next generation of scenarios for climate change research and assessment. *Nature*, 463, 747-756.
- National Oceanic and Atmospheric Administration (NOAA), 2016. National Ocean Service, Data Catalog, Retrieved from <https://data.noaa.gov/dataset/2009-2011-ca-coastal-california-topobathy-merged-project-digital-elevation-model-dem> on 09 January 2014.
- National Research Council (NRC), 2012. Sea-level rise for the coasts of California, Oregon, and Washington: past, present, and future. Committee on Sea Level Rise in California, Oregon, and Washington. The National Academies Press, Washington, 260 p.
- O’Reilly W.C., Guza, R.T., 1993. Comparison of two spectral wave models in the Southern California Bight. *Coastal Engineering*, 19(3):263–282.
- O’Reilly W.C., Guza, R.T., and Seymour, R.J., 1999. Wave prediction in the Santa Barbara Channel. Proc. 5th California Islands symposium, mineral management service, Santa Barbara CA, March 29–31.
- Pelnard-Considere, R., 1956. Essai de theorie de l’evolution des formes de rivage en plages de sable et de galets. 4th Journees de l’Hydraulique, Les energies de la Mer, Paris, 3(1), 289-298.
- Revell, D. L., Battalio, R., Spear, B., Ruggiero, P., & Vandever, J., 2011. A methodology for predicting future coastal hazards due to sea-level rise on the California Coast. *Climatic Change*, 109(1), 251-276.

- Reynolds, R.W., N.A. Rayner, T.M. Smith, D.C. Stokes, and W. Wang, 2002. An improved in situ and satellite SST analysis for climate. *J. of Climate*, 15, 1609-1625.
- Ris, R.C., Booij, N., and Holthuijsen, L.H., 1999. A third-generation wave model for coastal regions: Part II –Verification.: *Journal of Geophysical Research*, 104(C4), 7667-7682.
- Roelvink, J.A., 1993. Dissipation in random waves groups incident on a beach, *Coastal Eng.*, 19 (1-2), 127-150.
- Roelvink, D., Reniers, A., van Dongeren, A., de Vries, J.T. and McCall, R., 2009. Modeling storm impacts on beaches, dunes, and barrier islands, *Coastal engineering* 56 (11), 1133-1152
- Rogers, W.E., Kaihatu, J.M., Hsu, L., Jensen, R.E., Dykes, J.D., Holland, K.T., 2007. Forecasting and hindcasting waves with the SWAN model in the Southern California Bight. *Coastal Engineering*, 54, 1-15.
- Scripps Institution of Oceanography (SIO), 2016. Data retrieval by personal communication.
- Soulsby, R. L., 1997. *Dynamics of Marine Sands*, Thomas Telford, London.
- Storlazzi, C.D., Griggs, G.B., 1998. The 1997–98 El Niño and erosion processes along the central coast of California. *Shore and Beach* , 66(3):12–17.
- Tolman, H. L., and D. Chalikov, 1996. Source Terms in a Third-Generation Wind Wave Model. *Journal of Physical Oceanography*, 26, 2497-2518.
- Tolman, H.L., 2009. User manual and system documentation of WAVEWATCH III version 3.14. NOAA/NWS/NCEP/MMAB Technical Note 276:194 p
- Trenhaile, A. S., 2000. Modeling the development of wave-cut shore platforms. *Marine Geology*, 166(1), 163-178.
- Trenhaile, A. S., 2009. Modeling the erosion of cohesive clay coasts. *Coastal Engineering*, 56(1), 59-72.
- Trenhaile, A. S., 2011. Predicting the response of hard and soft rock coasts to changes in sea level and wave height. *Climatic Change*, 109(3-4), 599-615.
- U.S. Geological Survey (USGS), 2015. Coastal National Elevation Database (CoNED) Project – Topobathymetric Digital Elevatio Model. Sioux Falls, South Dakota. <https://lta.cr.usgs.gov>
- Vitousek, S. and Barnard, P.L., 2015. A non-linear, implicit one-line model to predict long-term shoreline change. In: P. Wang, J.D. Rosati and J. Cheng (Eds.), *The Proceedings of the Coastal Sediments 2015*, World Scientific, 14 pp., doi:10.1142/9789814689977_0215
- Walkden, M. J. A., & Hall, J. W., 2005. A predictive mesoscale model of the erosion and profile development of soft rock shores. *Coastal Engineering*, 52(6), 535-563.
- Walkden, M., & Dickson, M., 2008. Equilibrium erosion of soft rock shores with a shallow or absent beach under increased sea level rise. *Marine Geology*, 251(1), 75-84.
- Warrick, J.A., and Farnsworth, K.L., 2009, Sources of sediment to the coastal waters of the Southern California Bight, in Lee, H.J., and Normark, W.R., eds., *Earth science in the urban ocean--The Southern California Continental Borderland: Geological Society of America Special Paper 454*, p. 39-52.
- Yates, M. L., R. T. Guza, and W. C. O'Reilly, 2009. Equilibrium shoreline response: Observations and modeling, *J. Geophys. Res.*, 114, C09014, doi:10.1029/2009JC005359.

Appendix A: Downloadable data files

CoSMoS v3.0 Phase 2 URL:	https://www.sciencebase.gov/catalog/item/57f1d4f3e4b0bc0bebf139	
Description of CoSMoS v3.0 data <i>(per county unless stated otherwise)</i>	Format	File name (compressed)
CoSMoS Phase 2 flood hazard projections (flood extents, low-lying vulnerable areas, and flood uncertainty [max/min flood potential]): all SLRs for 1-year storm	shapefile	CoSMoS_v3_Phase2_1year_flood_hazards.zip
- all SLRs for 20-year storm	shapefile	CoSMoS_v3_Phase2_20year_flood_hazards.zip
- all SLRs for 100-year storm	shapefile	CoSMoS_v3_Phase2_100year_flood_hazards.zip
- all SLRs for background conditions	shapefile	CoSMoS_v3_Phase2_average_conditions_flood_hazards.zip
CoSMoS Phase 2 flood depth (centimeters) and duration (number hours of 24.85 hrs) projections: all SLRs for 1-year storm	GeoTIFF	CoSMoS_v3_Phase2_1year_flood_depth_and_duration.zip
- all SLRs for 20-year storm	GeoTIFF	CoSMoS_v3_Phase2_20year_flood_depth_and_duration.zip
- all SLRs for 100-year storm	GeoTIFF	CoSMoS_v3_Phase2_100year_flood_depth_and_duration.zip
- all SLRs for background conditions	GeoTIFF	CoSMoS_v3_Phase2_average_conditions_flood_depth_and_duration.zip
CoSMoS Phase 2 water level (total water level; relative to NAVD88) projections: all SLRs for 1-year storm	GeoTIFF	CoSMoS_v3_Phase2_1year_storm_water_elevation.zip
- all SLRs for 20-year storm	GeoTIFF	CoSMoS_v3_Phase2_20year_storm_water_elevation.zip
- all SLRs for 100-year storm	GeoTIFF	CoSMoS_v3_Phase2_100year_storm_water_elevation.zip
- all SLRs for background conditions	GeoTIFF	CoSMoS_v3_Phase2_average_conditions_water_elevation.zip
CoSMoS Phase 2 wave height projections: all SLRs for 1-year storm	GeoTIFF	CoSMoS_v3_Phase2_1year_storm_wave_height.zip
- all SLRs for 20-year storm	GeoTIFF	CoSMoS_v3_Phase2_20year_storm_wave_height.zip
- all SLRs for 100-year storm	GeoTIFF	CoSMoS_v3_Phase2_100year_storm_wave_height.zip
- all SLRs for background conditions	GeoTIFF	CoSMoS_v3_Phase2_average_conditions_wave_height.zip
CoSMoS Phase 2 ocean current projections: all SLRs for 1-year storm	GeoTIFF	CoSMoS_v3_Phase2_1year_storm_currents.zip
- all SLRs for 20-year storm	GeoTIFF	CoSMoS_v3_Phase2_20year_storm_currents.zip
- all SLRs for 100-year storm	GeoTIFF	CoSMoS_v3_Phase2_100year_storm_currents.zip
- all SLRs for background conditions	GeoTIFF	CoSMoS_v3_Phase2_average_conditions_currents.zip
CoSMoS-COAST Phase 2 projections of shoreline change for Southern California (all counties)	KMZ	CoSMoS_v3_Phase2_shoreline_projections.zip

CoSMoS Phase 2 projections of coastal cliff retreat for Southern California (all counties)	KMZ	CoSMoS_v3_Phase2_cliff_retreat_projections.zip
--	-----	--

Appendix B: Abbreviations, figures, and tables

BCC	Beijing Climate Center, China
CDIP	Coastal Data Information Program
CMIP5	Fifth Phase of the Coupled Model Inter-Comparison Project
D_m	mean wave direction
D_p	peak wave direction
DBDB2	Digital Bathymetric Data Base
GCM	global climate model
GFDL	Geophysical Fluid Dynamics Laboratory, NOAA, USA
GSHHS	Global Self-consistent Hierarchical High-resolution Geography Database
H_s	significant wave height
INMCM	Institute of Numerical Mathematics climate model, Russia
MIROC	Model for Interdisciplinary Research on Climate, Japan
NDBC	National Data Buoy Center, NOAA, USA
NOAA	National Oceanic and Atmospheric Administration, USA
RCP	representative concentration pathway
SLR	sea-level rise
T_m	mean wave period
T_p	peak wave period
WW3	WAVEWATCH-III wave model

Figures

Figure 1.	Map of study area and example photos of urbanized coastal sections.	8
Figure 2.	Schematic of the CoSMoS version 3.0 numerical model approach for simulation of coastal storm flooding	11
Figure 3.	Offshore wave height, wind, sea level pressure, and steric water level ranges employed in the modeled scenarios.....	12
Figure 4.	Estimates of steric water level contributions	15
Figure 5.	Tier II model extents.....	17
Figure 6.	Example profile types considered in merging cliff and shoreline model projections	22
Figure 7.	Schematic of approach used to estimate peak fluvial discharge rates associated with atmospheric storm patterns.....	25
Figure 8.	Idealized hydrograph.....	26
Figure 9.	Timing of events used in scenario model runs	28
Figure 10.	Illustration of method used to determine the flood extent at XBeach cross-shore profiles	29
Figure 11.	Schematic illustrating melding of Tier II and Tier III flood elevations and extents	30
Figure 12.	Schematic illustrating the combination of multiple model results from several storm simulations to attain one single map of local maximum values.	31

Tables

Table 1.	Models employed in CoSMoS.....	9
Table 2.	Tier II sub-model extents, number of grids, and grid resolutions	17
Table 3.	Fluvial discharge points included in Tier II model runs.....	19
Table 4.	Primary fluvial discharge.....	23
Table 5.	Sub-ordinate rivers and tributaries, drainage areas, and associated primary discharges	24
Table 6.	Gauging stations and details of each for development of unit hydrograph.....	26